



An experimental and modeling study on the reactivity of extremely fuel-rich methane/dimethyl ether mixtures

S. Porras^{a,*}, D. Kaczmarek^b, J. Herzler^c, S. Drost^a, M. Werler^a, T. Kasper^b, M. Fikri^c,
R. Schießl^a, B. Atakan^b, C. Schulz^c, U. Maas^a

^aInstitute of Technical Thermodynamics, Karlsruhe Institute of Technology, Karlsruhe, Germany

^bIVG, Institute for Combustion and Gas Dynamics – Thermodynamics, University of Duisburg-Essen, Duisburg, Germany

^cIVG, Institute for Combustion and Gas Dynamics – Reactive Fluids, University of Duisburg-Essen, Duisburg, Germany

ARTICLE INFO

Article history:

Received 10 April 2019

Revised 30 September 2019

Accepted 30 September 2019

Available online 2 November 2019

Keywords:

Fuel-rich reactions

Rapid compression machine

Shock tube

Flow reactor

Ignition delay time

Species concentration profiles

ABSTRACT

Chemical reactions in stoichiometric to fuel-rich methane/dimethyl ether/air mixtures (fuel air equivalence ratio $\phi = 1\text{--}20$) were investigated by experiment and simulation with the focus on the conversion of methane to chemically more valuable species through partial oxidation. Experimental data from different facilities were measured and collected to provide a large database for developing and validating a reaction mechanism for extended equivalence ratio ranges. Rapid Compression Machine ignition delay times and species profiles were collected in the temperature range between 660 and 1052 K at 10 bar and equivalence ratios of $\phi = 1\text{--}15$. Ignition delay times and product compositions were measured in a shock tube at temperatures of 630–1500 K, pressures of 20–30 bar and equivalence ratios of $\phi = 2$ and 10. Additionally, species concentration profiles were measured in a flow reactor at temperatures between 473 and 973 K, a pressure of 6 bar and equivalence ratios of $\phi = 2, 10$, and 20. The extended equivalence ratio range towards extremely fuel-rich mixtures as well as the reaction-enhancing effect of dimethyl ether were studied because of their usefulness for the conversion of methane into chemically valuable species through partial oxidation at these conditions. Since existing reaction models focus only on equivalence ratios in the range of $\phi = 0.3\text{--}2.5$, an extended chemical kinetics mechanism was developed that also covers extremely fuel-rich conditions of methane/dimethyl ether mixtures. The measured ignition delay times and species concentration profiles were compared with the predictions of the new mechanism, which is shown to predict well the ignition delay time and species concentration evolution measurements presented in this work. Sensitivity and reaction pathway analyses were used to identify the key reactions governing the ignition and oxidation kinetics at extremely fuel-rich conditions.

© 2019 The Authors. Published by Elsevier Inc. on behalf of The Combustion Institute.

This is an open access article under the CC BY-NC-ND license.

(<http://creativecommons.org/licenses/by-nc-nd/4.0/>)

1. Introduction

Recently, interest in co-generation and polygeneration processes for flexible conversion between different forms of energy and coupled production of valuable chemical species like syngas, acetylene (C_2H_2), and ethylene (C_2H_4) from cheap substances (especially methane) has increased [1–4]. The production of such chemicals is usually most efficient at very high equivalence ratios (typically exceeding $\phi = 6$), which are not used in conventional combustion processes. There is a lack of studies providing empirical data and validated chemical kinetics models for the ultra-rich regime.

The reaction kinetics of methane (CH_4), a suitable resource for polygeneration processes, have been extensively investigated in the last few decades by several authors. Hughes et al. [5] developed a comprehensive chemical mechanism to describe the oxidation of methane. The mechanism also accounts for the oxidation kinetics of other species like hydrogen, carbon monoxide, ethane, and ethene in flames as well as the autoignition problem in homogeneous mixtures. Petersen et al. [6], on the other hand, conducted an analytical study of CH_4/O_2 mixtures over a large range of conditions. A reaction mechanism was developed to supplement the high-pressure shock tube experiments on autoignition delay times [6]. Ignition delay times of similar mixtures have been reported by Brett et al. [7] and Gersen et al. [8] using a RCM and by Shukov et al. [9], who measured IDTs behind reflected shock

* Corresponding author.

E-mail address: sylvia.porras@kit.edu (S. Porras).

waves at elevated pressures between 3 and 450 bar and high initial temperatures. Measurements of species profiles describing the homogeneous partial oxidation of CH_4 have also been performed by different groups in high pressure flow reactors [10–13] and jet-stirred reactors [14], for a large range of reaction conditions covering pressures from 1 to 100 bar and temperatures between 600 and 1800 K. Most of the studies on methane combustion and oxidation have been focused on stoichiometric to slightly fuel-rich mixtures [5,6,14,15]. The thermodynamics and kinetics underlying methane pyrolysis at high temperatures have also been a point of interest for many research groups [16,17]. Some of them also studied the possibility of increasing the fuel conversion [18] or the yield of desired products [19,20] by investigating methane pyrolysis at temperatures higher than 1300 K.

Because the reactivity at ultra-rich conditions is generally lower compared to that of stoichiometric fuel/air mixtures, reaction enhancers are often used to initiate the reaction under practically accessible pressures and temperatures [13]. DME (dimethyl ether, CH_3OCH_3), having a high cetane number, low sooting tendency, and good availability, is a suitable ignition enhancer [21–24]. DME is also used in gas turbines as an additive or alternative to natural gas [25,26]. Several experimental [22–24,27–33] and theoretical [34–36] studies have described the reaction of pure DME under a wide range of conditions: Curran et al. investigated the pyrolysis and oxidation of DME experimentally under highly diluted conditions for equivalence ratios between 0.7 and 4.2 [23,27]. Zhao et al. [37] performed a theoretical and experimental analysis of the unimolecular decomposition of DME applying a hierarchical methodology to develop a high-temperature model describing pyrolysis and oxidation of DME at $\phi \leq 2.5$. Dagaut et al. [22,28] studied the oxidation of DME by measuring concentration profiles of reactants, intermediates, and products in a jet-stirred reactor at 10 atm, $0.2 \leq \phi \leq 1$ and in a temperature range of 550–1100 K as well as ignition delay times in a shock tube at 1200–1600 K, 3.5 atm of pressure and equivalence ratios between $\phi = 0.5$ –2. They also proposed a reaction mechanism. Shock tube measurements have also been performed to study the self-ignition of DME/air mixtures under engine relevant conditions [30] as well as its thermal dissociation [38] and pyrolysis [39]. Zheng et al. [31] determined experimentally the ignition temperature of DME/ N_2 mixtures in counterflow diffusion flames; experiments were carried out varying the DME concentration from 5.9 to 30% in a pressure range of 1.5–3 atm. Other experiments including measurements of DME flame speeds have been published by de Vries et al. [40] and Daly et al. [32]. On the other hand, Amano and Dryer [41] studied the ignition enhancing effect of DME in CH_4 /air mixtures by adding small amounts of DME to the gas mixture. They found that a small amount of DME had a stimulating effect on autoignition of CH_4 /air mixtures [41]. Similar conclusions were made by Chen et al. [42] and Tang et al. [43], who measured the effect of DME on methane mixtures at high temperatures [42] and mole fractions of DME in the mixture from 1 to 50% [43]. The effect of adding dimethyl ether to methane with respect to the laminar flame speed was studied experimentally and numerically by Lowry et al. [44] over a range of initial pressures from 1 to 10 atm for different fuel blends ranging from 60% CH_4 /40% DME to 80% CH_4 /20% DME in volume. The influence of DME in the formation of soot and polycyclic aromatic hydrocarbons (PAH) on methane fuel mixtures was also a topic studied by Yoon et al. [45]. They found, that the formation of soot and PAH significantly decreases for the mixtures of DME with methane, ethane and propane, while a higher presence of these compounds was observed in DME/ethylene mixtures compared to mixtures of the fuel without additive [45].

Detailed and validated chemical kinetics models describing CH_4 /DME mixtures are readily available for stoichiometric or near-stoichiometric conditions. It is unclear whether they are also suit-

able as predictive tools in the ultra-rich regime. Burke et al. [46] developed a reaction mechanism for methane, DME, and their mixtures which has been validated for mixtures in a wide range of temperatures and pressures at $\phi = 0.3$ –2.5. Hashemi et al. [47], on the other hand, presented a chemical kinetic model to describe the pyrolysis and oxidation of DME and its mixtures with methane at high pressures (50–100 bar), intermediate temperatures (450–900 K) and equivalence ratios of $\phi = 0.06$, 1 and 20 studied in a laminar flow reactor. Other mechanisms like the DME mechanisms of Zhao et al. [37] or Fischer et al. [23] were not developed to describe methane oxidation.

To provide a reaction mechanism tailored for polygeneration-relevant conditions, a new detailed kinetics mechanism including CH_4 /DME was developed based on existing mechanisms for methane pyrolysis [48] and oxidation [49], and the DME mechanism of Zhao et al. [37]. Hidaka et al. [48] developed a chemical kinetic model able to predict accurately the pyrolysis and oxidation of methane at elevated temperatures, which are needed to initiate the reaction of methane without addition at lower presence of oxygen in the initial mixtures. On the other hand, Heghes [49] presented a C_1 – C_4 elementary reaction mechanism, which accurately describes stoichiometric to slightly fuel-rich mixtures ($\phi < 2$) of CH_4 and air. The combination of these should be able to describe the oxidation of methane at extremely fuel-rich conditions without missing any significant reaction pathway. The DME sub-mechanism of Zhao et al. [37] was included, as DME is used as reaction enhancer in this study in order to perform experiments at engine relevant conditions.

Experimental results of the oxidation of CH_4 /DME mixtures were carried out in a rapid compression machine, a high-pressure shock tube and in a flow reactor. The three experimental setups present different timescales and operational characteristics providing valuable experimental data in a large range of initial conditions, namely temperature and pressure, that complements each other. The information about the reactivity of the mixtures through ignition delay times and species profiles is of great importance for mechanism validation and a comprehensive study of the kinetics taking place at low and high temperatures.

In the following, experimental results of the oxidation of CH_4 /DME mixtures are described. Then, the development of the new kinetics model is outlined. Finally, comparisons of experimental data with model predictions based on the new reaction mechanism are presented.

2. Experiments

2.1. Rapid compression machine

Measurements of ignition delay times and species concentration profiles were carried out in a Rapid Compression Machine (RCM) and in a Rapid Compression-Expansion Machine (RCM), respectively. The RCM facility has been described previously by Werler et al. [50]. It consists of a temperature-controlled cylinder-piston device in which the piston compresses the cylinder load, before being locked at top dead center (TDC). A creviced piston was used which can swallow the boundary layer peeling off the cylinder wall [50], providing more homogeneous in-cylinder thermal conditions compared to a standard piston. Pre-compression pressures were measured using a capacitance manometer (MKS Baratron 121A). This, combined with a pressure transducer (Kistler 6061 B) attached to the cylinder head, enables the determination of time-resolved absolute pressure traces. Pre-compression temperatures were measured with a type-K thermocouple. The cylinder head was equipped with an optical access via a quartz glass fiber. A photomultiplier (Hamamatsu H10722-210) equipped with a short pass filter (450 nm) was used for time-resolved chemiluminescence

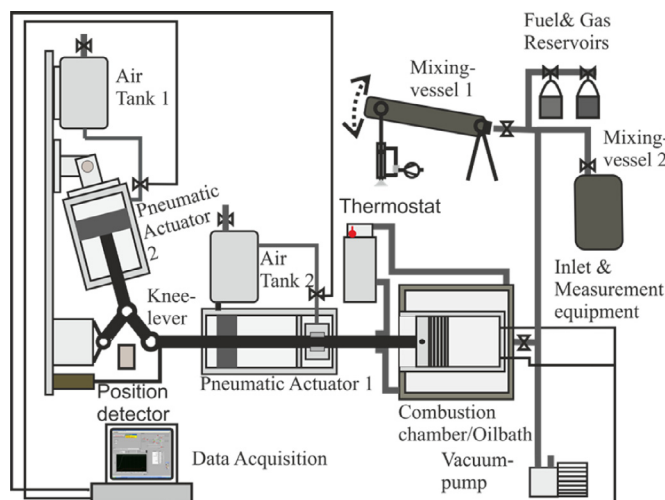


Fig. 1. Rapid compression machine setup.

detection. During the measurement, a potentiometric position sensor (Burrster type 7812) recorded the piston position. A mixing vessel was connected to the RCM, in which a homogeneous mixture of the test gas was created and stored. A scheme of the RCM is shown in Fig. 1.

In RCM ignition delay time measurements, the time span between the moment where the piston reaches TDC and the inflection point of the pressure trace (point at which the pressure gradient reaches a maximum) due to first-stage ignition as well as main (second-stage) ignition were defined as the first and main ignition delay time, respectively. Values of temperature and pressure immediately after compression were assigned to the measured IDT. The post-compression pressure p_c was measured and the corresponding temperature T_c was calculated from p_c and pre-compression values p_0 and T_0 using the isentropic-core assumption [51,52].

To obtain a desired combination of temperature and pressure at TDC in an RCM experiment, the initial temperature, compression ratio, and composition of the inert gas in the mixture were varied. The accumulated uncertainties of the measurement equipment caused maximum uncertainties of $\pm 1.4\%$ and $\pm 0.71\%$ in the determination of T_c and p_c , respectively.

The RCEM is an extension of the RCM, which adds a controlled expansion phase to the conventional RCM process [51,53,54]. The driving system of the experimental setup is shown in Fig. 2. After compression, the gas mixture is held in an isochoric state for a controllable hold time τ_{hold} . After this, the piston is retracted, resulting in a rapid expansion of the trapped gas. The quick decrease of temperature and pressure during expansion largely freezes the ongoing chemical reactions, allowing convenient subsequent sampling and *ex situ* analysis of the expanded gas, without requiring high-speed measurement devices. The species measurement system attached to the facility features a micro gas chromatograph (Agilent 490 Micro GC) with three chromatography columns, namely MS5A, PPU, and a CP-Sil 5CB, with their respective thermal conductivity detector, allowing the analysis of permanent gases as well as many hydrocarbons up to C_{10} species. The compression-expansion cycle comprised in the RCEM, combined with the adjustable hold time and post-compression probe sampling capability, allows monitoring the evolution of species concentrations during reaction as a function of hold time.

Figure 2 highlights the RCEM operation; in particular, Fig. 2b depicts some pressure profiles which were taken from subsequent experiments with identical initial conditions, but with different hold times.

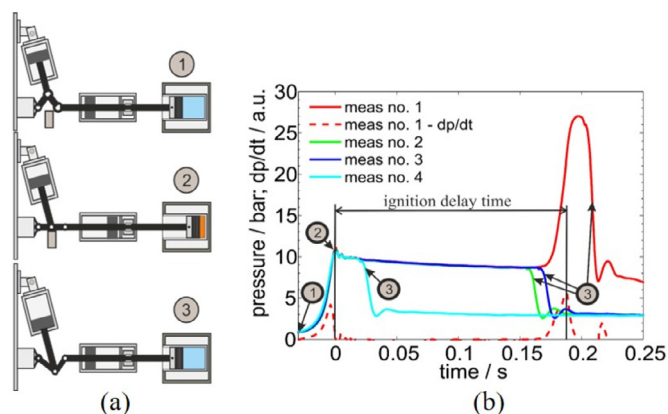


Fig. 2. RCEM driving system. (a) Illustration of the RCEM operation (b) Experimental pressure traces during ignition and for different τ_{hold} . The initial mixture in the reaction chamber (1) is compressed and held in an isochoric state (2) for a controlled hold time, at which the piston is pulled back, expanding the in-cylinder gas (3). The hold time can be varied for obtaining information about the product composition after variable reaction times.

In these measurements, uncertainties related to species profiles are caused mainly by the GC calibration gas and the measurement equipment, obtaining relative uncertainties of 3.8–9.3% for the inlet fuel and main products (e.g., CO, H_2) and between 14.3 and 15.5% for the C_2 -products [55].

2.2. Shock tube

Measurements of ignition delay times and end products were carried out in a high-pressure shock tube with a constant inner diameter of 90 mm and lengths of the driver and driven sections of 6.4 and 6.1 m, respectively. Allowable post-ignition peak pressures are 500 bar and the maximum test time is extended up to 12–15 ms by driver-gas tailoring. Helium was used as the main driver gas component and argon was added to match the acoustic impedance of the driver gas with the one of the test gas. The driver gas was mixed *in situ* by using two high-pressure mass flow controllers. The driver gas composition depends on the test gas mixture composition and the Mach number was calculated prior to the experiment. For the calculation, formulas by Oertel [56] and Palmer and Knox [57] were used.

Test gas mixtures were prepared manometrically in a mixing vessel and stirred for one hour to ensure homogeneity. DME was purified before use by freezing with liquid nitrogen and removing remaining gases (e.g., N_2) by pumping.

The temperature and pressure behind the reflected shock waves were computed from the incident shock velocity using a one-dimensional shock model with an estimated temperature uncertainty of $T < 15$ K. The shock velocity was measured over two intervals using three piezoelectric pressure transducers at different distances from the end flange. Band pass-filtered (413 ± 5 nm) emission from CH^* chemiluminescence was monitored through a window in the sidewall 15 mm from the end flange with Hamamatsu 1P28 photomultiplier tubes. The pressure was recorded at the same position using a piezoelectric pressure transducer. Ignition delay times were defined as the interval between the rise in pressure due to the arrival of the reflected shock wave at the measurement port and the extrapolation of the steepest increase in CH^* emission to its zero level on the time axis (Fig. 3).

Gas samples were taken with a fast opening valve integrated in the end wall (Parker Hannifin Pulse Valve Series 9) connected to a 50 ml vessel. The valve was operated with a Parker Hannifin Iota One driver. The valve was opened 10 ms after the arrival of the reflected shock wave for 10 ms. The samples were analyzed

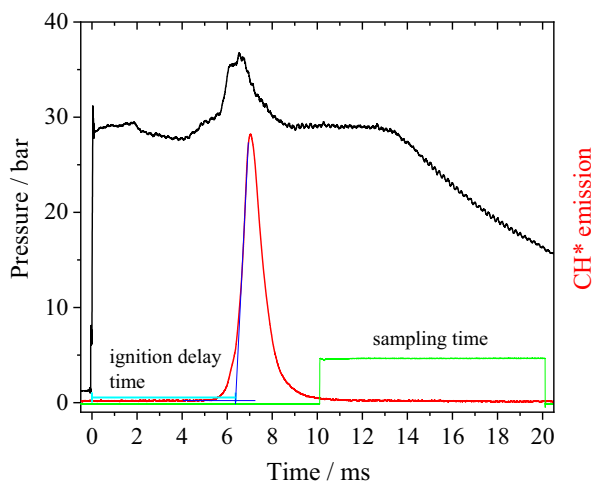


Fig. 3. Temporal variation of pressure (black) and CH^* emission (red) measured in the shock tube with a $\text{CH}_4/\text{DME}/\text{air}$ mixture ($\phi = 10$) at 28.5 bar and 735 K. (For interpretation of the references to color in this figure legend, the reader is referred to the web version of this article.)

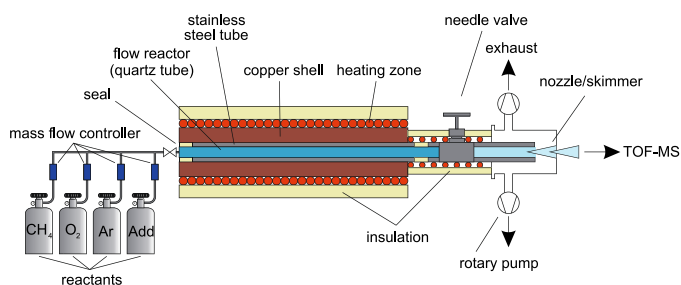


Fig. 4. Experimental setup of the plug-flow reactor with TOF-MS.

with gas chromatography and mass spectrometric analysis (GC/MS, Agilent Technologies GC System 7890 A, MSD 5975C with a J&W HP-PLOT Q column). Each mixture used in the experiments contained 2% Ne as internal concentration standard and all concentrations were determined relative to the internal standard. Mixtures of the expected products and the internal standard were prepared manometrically in a mixing vessel and used for calibration of the GC/MS system.

2.3. Flow reactor

Species concentration profiles were measured in a plug-flow reactor displayed in Fig. 4.

It consists of a 65 cm quartz tube embedded in a stainless-steel tube. The stainless-steel tube, which in turn is surrounded by two copper shells for improving temperature homogeneity, acts as a pressure shell. The gap between the quartz and the stainless-steel tube is sealed with teflon tape to prevent reactants from entering the gap. Heating tapes are wrapped around the copper shells and used to provide the heat that is necessary to initiate the reaction. Due to this arrangement, the temperature profile along the reactor consists of a 45 cm long isothermal zone and very steep temperature increases and decreases at the inlet and the outlet of the reactor. To ensure that no condensation of product species takes place at the reactor outlet, the path behind the reactor is also heated by heating tapes to 393 K. Individual reactant flows are regulated by mass flow controllers (MKS) and mixed before entering the reactor. For the analysis of the species at the outlet, the reactor is coupled with a molecular-beam time-of-flight mass spectrometer (TOF-MS) via a heated needle valve and three pressure stages. The mass res-

Table 1
Investigated mixture compositions (mol%).

	No.	%CH ₄	%DME	%O ₂	%Ar	%N ₂	%Ne	ϕ
RCM	1	8.18	0.91	19.09	–	71.82	–	1.0
	2	15.00	1.67	17.50	–	65.83	–	2.0
	3	33.75	3.75	13.13	49.38	–	–	6.0
	4	37.06	4.12	12.35	46.47	–	–	7.0
	5	45.00	5.00	10.50	39.50	–	–	10.0
	6	54.00	6.00	8.40	31.60	–	–	15.0
	7	13.54	1.52	5.30	79.55	–	–	6.0
	8	13.43	1.49	4.47	80.60	–	–	7.0
	9	14.90	1.66	3.48	79.97	–	–	10.0
	10	16.85	1.87	2.62	78.65	–	–	15.0
Shock tube	11	15.83	0.83	17.08	–	66.25	–	2.0
	12	12.57	3.14	17.28	–	67.01	–	2.0
	13	44.40	4.94	10.38	–	38.23	2.00	10.0
RCEM	14	15.00	1.67	17.50	–	65.83	–	2.0
	15	33.75	3.75	13.13	44.44	4.94	–	6.0
	16	45.00	5.00	10.50	35.55	3.95	–	10.0
Flow reactor	17	4.69	0.25	5.06	90.00	–	–	2.0
	18	4.39	0.49	5.12	90.00	–	–	2.0
	19	7.89	0.41	1.70	90.00	–	–	10.0
	20	7.44	0.83	1.74	90.00	–	–	10.0
	21	8.62	0.45	0.93	90.00	–	–	20.0
	22	8.14	0.90	0.95	90.00	–	–	20.0

olution of the TOF-MS is $m/\Delta m = 2000$. After entering the ionization chamber of the TOF-MS, the product gas is ionized by electron ionization (17 eV kinetic energy) to avoid excessive fragmentation.

Species mole fractions in the reacting argon-diluted $\text{CH}_4/\text{DME}/\text{O}_2$ mixtures were measured at the exit of the plug-flow reactor at various temperatures and equivalence ratios. Prior to the experiments, calibration measurements using self-mixed binary cold gas mixtures were carried out. The resulting relative uncertainties in calculated mole fractions of calibrated and detected species are 10%. The uncertainties were evaluated based on a Gaussian error propagation law taking all relevant sources of error into account. A detailed description of the experimental setup can be found in Refs. [58,59].

2.4. Investigated experimental conditions

All investigated mixtures in this study are listed in Table 1. IDTs of $\text{CH}_4/\text{DME}/\text{air}$ mixtures were measured in the RCM at equivalence ratios of $\phi = 1, 2, 6, 7, 10,$ and 15 , for $T_c = 600\text{--}1050\text{ K}$ and $p_c = 10\text{ bar}$ using DME as additive with a concentration of 10 mol% in the fuel. The equivalence ratio was defined treating CH_4 and DME as fuels and O_2 as oxidizer, i.e., assigning the O-atom in DME to the fuel, not to the oxidizer. For investigations in the $\phi = 6\text{--}15$ range, two sets of IDT measurements were conducted for: (i) mixtures with air: 79:21 Ar/ O_2 , and (ii) mixtures with high Ar dilution: 95:5 Ar/ O_2 to reach high post-compression temperatures corresponding to mixtures 3–6 and 7–10 in Table 1, respectively.

IDTs were also measured in a shock tube for $\text{CH}_4/\text{DME}/\text{air}$ mixtures at $\phi = 2$ and 10 at 20 bar (mixtures 11–12 in Table 1) and 30 bar (mixture 11 and 13) and temperatures between 630 and 1500 K (mixtures 11–13). The DME concentration was varied from 5 to 20 mol% with respect to the fuel. End products were determined only for mixture 13 ($\phi = 10$) at 30 bar. For this case, 2 mol% neon was added to the mixture as indicated in the section above.

Product species concentrations after variable reaction times were measured in the RCEM for the mixtures 14, 15, and 16 (Table 1). These mixtures represent the equivalence ratios $\phi = 2, 6,$ and 10 , respectively; mixture 15 and 16 feature identical amounts of fuel and oxygen as mixtures 3 and 5 with the difference that 10% of argon was replaced by nitrogen. This provided a GC-

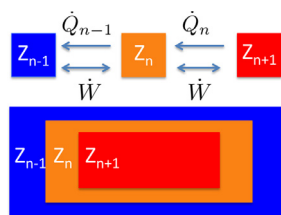


Fig. 5. Schematics of the multi-zone model.

detectable inert gas, thus the reaction-induced change of moles in the mixture could be monitored for further comparison with simulations. No significant chemical conversion could be observed in our experiments at $\phi = 15$ so that the data for these conditions are not presented here.

In the plug-flow reactor, species mole fractions as function of temperature in the isothermal zone were measured for the reacting $\text{CH}_4/\text{DME}/\text{O}_2$ mixtures at $\phi = 2, 10,$ and 20 for $473\text{--}973\text{ K}$ and 6 bar . A high dilution of argon (90%) in the mixtures was needed to minimize the temperature increase due to exothermal reactions. Simulations of the system using the shear flow model of ChemKin Pro 19.2 to include heat transfer from the wall to the gas as well as the heat release due to exothermal reactions show that typically the temperature increase by reactions is a very localized phenomenon and limited to less than 60 K , if the dilution is $\geq 90\%$. Therefore, the effect on the mole fractions at the outlet of the reactor can be neglected. The amount of DME was varied between $5\text{ mol}\%$ (mixtures 17, 19, and 21) and $10\text{ mol}\%$ (mixtures 18, 20, and 22) related to the fuel for each equivalence ratio.

3. Modeling of experimental data

3.1. Simulation of RCM and RCEM data

Simulations of IDTs were performed using a homogeneous reactor model based on an adiabatic-core hypothesis for all mixtures [51]. A volume trace describing the compression and expansion of the core gas was used as an input for the simulations to account for the compression phase and the heat loss. For each mixture, this volume trace was derived from the pressure trace of RCM experiments without reaction, as described in Mittal and Sung [51]. For these non-reacting measurements, O_2 was replaced by the same molar amount of N_2 , yielding an inert mixture with similar isentropic exponents and thermal diffusivities as the corresponding reacting mixture [60].

The adiabatic-core model is suitable for the reproduction of IDTs since it can describe the reactions taking place in the core of the reaction chamber between compression and ignition, typically a time span in the range of a few to 100 ms . The reaction core represents a small portion of the total reaction volume only. It can reach temperatures that are significantly higher than in the rest of the reaction chamber. In the course of reaction, this thermal inhomogeneity causes a compositional inhomogeneity through the strongly temperature-dependent reaction rates.

A realistic description of the temporal evolution of the product species requires consideration of the entire reaction volume as well as the heat transfer from the core to the rest of the reaction chamber [60]. A multi-zone model was used to account for this effect. This model assumes that the reaction chamber consists of multiple zones that are arranged in an onion-like fashion. Within every zone, all scalar fields are assumed to be spatially uniform but may differ from zone to zone. The zones have the same instantaneous (but temporally variable) pressure and can exchange heat and expansion work, but not mass. A scheme of the model is shown in Fig. 5.

The heat exchanged between adjacent zones or the outermost zone and the wall is calculated from their temporally varying contact surface, the temperature difference between adjacent zones, and two heat-transfer coefficients. The heat-transfer coefficients between the zones are assumed to be equal while a second one is calculated for the heat flow taking place between the outermost zone and the wall. These values are calibrated by pressure traces measured in non-reactive RCEM experiments. The multi-zone model can then treat transient cylinder volume traces and therefore also the compression-expansion phases of the RCEM, allowing the zones to develop different chemical progress according to the thermodynamic conditions in each zone. The measured overall composition in the RCEM is modeled by the mass-averaged composition over all zones.

The number of zones required for a realistic description of the heat transfer was determined by comparing experiment and simulation: Pressure profiles of unreactive experiments were compared to pressure profiles predicted by multi-zone simulations which received the experimental cylinder volume trace $V_{\text{cyl}}(t)$ as an input. Simulations using 13 zones were found to be sufficient to match the experimental data well. A more detailed description of the multi-zone model and its respective validation can be found in Refs. [55,60].

3.2. Simulation of shock tube data

The simulations of the shock tube data are based on the observed pressure increase of $1\%/ms$ ($\phi = 10$) or $5\%/ms$ ($\phi = 2$) for the first 2.8 ms to account for the facility effect [61]. This pressure increase was determined by measurements with inert gas mixtures that exhibit no heat release during the measurement time. After the first 2.8 ms , when the reflected shock wave passed through the contact surface, no further pressure increase was typically observed (Fig. 3). The simulations were performed with a constant-pressure assumption considering a temperature increase by the gas dynamic adiabatic and isentropic compression measured in inert mixtures. For the simulation of the product formation the cooling after the measurement time was also considered based on the measured pressure profiles and adiabatic and isentropic expansion [61].

3.3. Simulation of flow reactor data

The measured flow reactor data was simulated via a plug-flow model [62] that assumes invariant gas composition and velocity in radial direction, reducing the problem to a one-dimensional approach without the influence of heat transfer. The plug-flow is an efficient model for flow reactor simulations where the gas temperature and pressure along the reactor can be assumed to remain constant during the reactions process. Simulations were performed using the geometric specifications of the flow reactor as well as the gas temperature profiles measured inside of the reactor prior to the experiments with similar gas flows as inputs. The simulations used the complete temperature profile along the center line of the axis including the isothermal zone as well as the zones of temperature rise and decrease at the reactor inlet and outlet; the resulting mole fractions at the outlet were compared between simulation and experiment.

4. Chemical kinetics model

Modeling of extremely fuel-rich conditions relevant in polygeneration processes requires reaction mechanisms developed especially for the prediction of the reaction kinetics for these mixture compositions. Unfortunately, chemical kinetics models found in the literature describing the combustion and oxidation of CH_4/DME

mixtures have been developed and validated to predict the kinetics of mixtures up to $\phi < 2.5$ [27,37,46]. No dedicated mechanism describing very high equivalence ratios was found in the literature, motivating the development of a new chemical kinetics model. Another motivation for the development of a dedicated reaction mechanism for polygeneration applications is that the mechanism can be comparatively small so that it is well suited to further manipulation, e.g., reduction procedures. Polygeneration conditions have not been investigated in detail yet and an optimization of reaction conditions using efficient simulation and optimization procedures [4] is needed to obtain reasonable product yields in technical polygeneration reactors, e.g., piston engines [3].

The new assembled model is based on existing detailed mechanisms describing stoichiometric to slightly fuel-rich ($\phi = 1-2$) combustion and pyrolysis of methane as well as the oxidation of DME/air mixtures. The new model aims at predicting IDTs and species concentration–time profiles of CH₄/DME/air mixtures at $\phi \geq 6$.

Sensitivity and reaction flow-rate analyses were carried out for different temperatures and mixture compositions in order to identify the rate-limiting reactions in the range covered by the experimental data. Reaction rate constants of some of these reactions were modified based on either previous publications by other authors [27,46,63,64] or a chemical kinetic database found in the literature [65]. Physical soundness of these modifications was a concern, so all changes were performed only within the documented experimental uncertainty range. A detailed description of the mechanism construction is given in the subsections below.

The resulting polygeneration mechanism (PolyMech) consists of 558 elementary reactions among 83 species. A description of the key reactions and reaction pathways needed for the prediction of the regimes studied in this work as well as the mechanism validation against ignition delay times and species profiles measured in the experimental setups mentioned above are presented in the following section. The mechanism with its corresponding thermodynamic data file is attached to this paper as supplement.

4.1. Sub-mechanism for methane oxidation

Due to the lack of reaction mechanisms available in the literature for the description of methane oxidation at very high equivalence ratios ($\phi \geq 6$) and the temperature ranges covered in this work, a new model was assembled based on existing mechanisms developed for combustion and high temperature pyrolysis of CH₄. The reaction model published by Heghes [49,66] describing stoichiometric to slightly fuel-rich mixtures ($\phi < 2$) was merged with the pyrolysis mechanism of Hidaka et al. [48] for this purpose. Both were constructed for predictions of CH₄/air mixtures in a wide temperature range. The combination of these were carried out primarily by taking the pyrolysis and non-O₂ reactions from Hidaka's mechanism [48] as well as the oxidation steps from Heghes [49] avoiding the duplication of reactions. The resulting kinetics model was complemented with reactions not included in the previous mechanisms describing pyrolysis and oxidation of acetylene [67], vinylacetylene [68], propyne and allene [69], as well as the ethanol sub-mechanism presented by Marinov [70].

Rates of methane reactions were modified to allow the prediction at extremely fuel-rich conditions. Rates for the H-abstraction from methane by hydroperoxyl (HO₂) used in this work were derived by Scott and Walker [71] which proposed a non-Arrhenius form for the expression of reaction rate constant using a temperature exponent of 2.5, based on calculations applying the method of Chen and Bozzelli [72]. The expression for the reaction rates was obtained implementing the experimental values measured by Baldwin et al. [73] together with an A factor per C–H bond identical to the one measured for the reaction between HO₂ and ethane.

The authors reported an uncertainty of the reaction rate of 1.41 between 600 and 800 K rising up to 5 at 2000 K. For the H-abstraction reaction from CH₄ by H atoms, the recommended values presented by Baulch et al. [63] were implemented. These are shown to be in good agreement with the expression presented by Cohen [74] and Sutherland et al. [75]. Sutherland et al. derived their rate expression by combining their own measurements with the one performed by other authors [63]. The pre-exponential factor of these reactions were reduced by 30% and 50%, respectively, which is within the uncertainty limits reported by the authors [73,75] and are in accordance with the expressions presented by Metcalfe et al. [76] and Burke et al. [46]. Heghes [49] and Baulch et al. [63] proposed the same reaction rates for the reaction of methane with oxygen, which were estimated based on the H-abstraction reaction from HCHO by O₂. Calculations of the reverse reaction using ab initio molecular orbital theory and variational RRKM theory performed by Zhu and Lin [77] are consistent with the expression presented by Heghes [49]. The combination of the theoretical values of Zhu and Lin [77] together with thermodynamic data were implemented, giving reaction rate values with an uncertainty of 3 to 5 over the range of 500–2000 K [63]. The pre-exponential factor of the latter reaction was modified by a factor of 1.65, resulting in reaction rates similar to the values published by Burke et al. [46], Hidaka et al. [48] and Reid et al. [78], who performed simulations of ignition delay times for methane/air mixtures.

Methyl radicals (CH₃) are mostly produced by H abstraction from methane. These radicals recombine quickly to produce ethane (C₂H₆) triggering a sequence of H-abstraction reactions to stable species such as ethylene (C₂H₄) and acetylene (C₂H₂). The rates of the methyl recombination reaction were replaced by the values recommended by Baulch et al. [63] based on the experimental data of Gläzer et al. [79], Hippler et al. [80], Slagle et al. [81] and Macpherson et al. [82] at high temperatures and the measurements of Walter et al. [83] for the low temperature range. While the expression for the low-pressure limit presented by Baulch et al. is in accordance with the values published by Blitz et al. [84], the pre-exponential factor of the high-pressure limit was lowered by a factor of 1.5 to meet the recently proposed rates presented by Blitz et al. [84], who performed an analysis of the reaction rates using revised cross sections and second order master equation to determine their proposed values. Rates of C₂H₅ dissociation to C₂H₄ and H were replaced by the coefficients included in Heghes' reaction mechanism [49], presenting reaction rates, being a factor of 2.56 higher for the high-pressure limit and a factor of 0.57 lower for the low-pressure limit compared to the values from Hidaka's reaction mechanism [48]. The reaction rates presented by Heghes [49] are the same as the ones proposed in the analysis performed by Baulch et al. [63], which are based on a large library of experimental data regarding the temperature range of 200–1100 K.

Formaldehyde (CH₂O) has been identified as an important intermediate in the oxidation and combustion of methane [46,48]. Reactions comprising the H abstraction from CH₂O by several radicals have shown to be very important for the accurate predictions of IDTs and of CO concentration–time profiles. Rates of the H-abstraction reaction from formaldehyde by H radicals were taken originally from the mechanism of Heghes [49]. The reaction rate coefficients presented by Heghes are the result of a least squares 3 parameter fit of low and high temperature measurements carried out by other authors [85–87]. The resulting expression has a reported uncertainty factor of 1.25 at 290 K increasing up to 3.2 with increasing temperature. Expressions derived by other authors [63,88] have shown to be in a good agreement with the rates included in Heghes' mechanism [49] at ambient temperatures. Nev-

ertheless, these have shown some discrepancies with increasing temperature. The pre-exponential factor of this reaction was modified within its reported reliability range. At high temperatures, HO₂ radicals are able to abstract an H atom from formaldehyde, while at temperatures near 298 K, HO₂ molecules tend to be added forming HOCH₂OO. Rates for the H-abstraction were taken from the values reported by Eiteneer et al. [89], who derived the expression fitting a complex mechanism and considering measurements presented by other studies. The derived values were modified within their uncertainties, resulting in similar rates as the ones published in the mechanism of Burke et al. [46]. The rates for the formation of methane molecules from the H-abstraction reaction from CH₂O by methyl radicals were selected from the recommended values of Baulch et al. [63]. These represent the best fit of several rate coefficient measurements [90–92] together with reviews and evaluations carried out by Kerr and Parsonage [93]. A modification of the A factor of this reaction was made, giving similar values as the reported ones by Burke et al. [46]. Finally, the reaction rates of the reaction of CH₂O with OH were obtained from the reported values by Warnatz [94]. These were increased in order to meet the values presented by other authors [95] at low temperatures.

Reactions comprising the oxidation and thermal dissociation of ethanol were substituted by the sub-mechanism of Marinov's mechanism [70] that was specifically developed to describe the reaction of ethanol. Ethanol reacts to form three isomeric radicals by losing an hydrogen atom, with 1-hydroxyethyl (CH₃CHOH) being the primary product [96]. Rates of ethanol reactions with CH₃, OH, and HO₂ radicals were modified following the preferred values presented by Baulch et al. [63]. CH₃CHOH, the main product of ethanol decomposition and also formed by isomerization of CH₃CH₂O through an H shift, produces CH₃CO and CH₂CHO by several H abstractions. The pathway towards CH₃CO has been considered more important in contrast to the one towards CH₂CHO in several studies [84]. Reactions of acetaldehyde with CH₃ and H radicals forming CH₃CO were adapted according to the recommendation by Baulch et al. [63].

The formation of hydroxyl from H + O₂ and H₂ + O reactions are extremely important in the hydrogen sub-mechanism (especially the first one), since these dominate and determine the reaction velocity of hydrocarbon fuel undergoing oxidation at temperatures higher than 1000 K. For temperatures lower than 1000 K (also depending on the system pressure) the formation of OH-radicals competes with the production of HO₂ from the reaction of H + O₂. Reaction rates for the formation of hydroxyl radicals presented in the methane mechanism of Hidaka et al. [48] were reduced by 20% to meet the newly published values from the hydrogen mechanism of Kéromnès et al. [64]. They adopted the measured rate constants from Hong et al. [97] and Sutherland et al. [106] respectively. The first author combined their H₂O absorption measurements behind reflected shock waves with those reported by Masten et al. [107], while the second one combined a flash photolysis shock tube technique with an atomic resonance absorption spectroscopy to obtain their expression for the reaction rates. On the other hand, the reaction rates of H + O₂ to hydroperoxyl radicals, important for the low temperature oxidation were adopted from the reaction mechanism of Kéromnès et al. [64], who combined the low pressure rate limit constant from Bates et al. [98] with the high pressure limit from Fernandes et al. [99] to match their RCM and shock tube measurements. The pre-exponential factor of the low-pressure limit was increased in order to obtain better prediction of the presented low temperature RCM experimental data for equivalence ratios between $\phi = 6$ –15. The formation and consumption of hydrogen peroxide (H₂O₂) also play an important role in the determination of IDTs and species concentration–time profiles. The thermal dissociation of H₂O₂ is one of the main production sources of OH radicals

and a highly sensitive reaction. Dissociation rates of H₂O₂ were obtained from the theoretical analysis carried out by Troe [100], who reviewed experimental data to obtain a pressure dependent rate constant expression for this reaction. The rates presented by Troe have been implemented by other authors showing good results in the prediction of ignition delay times at different pressures [64]. The formation rates of H₂O₂ by recombination of two HO₂ radicals were adopted from the studies carried out by Hippler et al. [101]. Hippler et al. investigated the reaction rates of this reaction experimentally and obtained a rate constant expression by combining their high pressure measurements with evaluated low temperature data. The rate constants recommended by Hippler et al. [101] were slightly increased within their experimental uncertainties. The recombination reaction of HO₂ concur in the intermediate temperature oxidation range with the reaction of HO₂ with H₂ to produce one hydrogen peroxide molecule and a hydrogen atom. Rates of the latter reaction were adopted from Ellingson et al. [102], who performed canonical variational transition state theory calculations with multidimensional tunneling for obtaining the proposed reaction rate expression.

4.2. DME sub-mechanism

As mentioned before, a small amount of DME was added to the fuel mixtures to enable methane conversion at low temperatures. Methane is relatively inert at low temperatures, which is more pronounced at high equivalence ratios because of the lack of oxygen (and thus heat release) in the mixture. DME was also added to PolyMech as a reaction enhancer. Its sub-mechanism represents a key element in the kinetics description of the mixtures covered in this study. DME reacts easily with O₂ at low temperatures providing the conditions (formation of radicals and increasing the temperature of the gas mixture) needed for methane to react. Zhao's DME sub-mechanism [37] was selected for the description of DME decomposition and oxidation. However, several reaction rates were modified or substituted by the ones presented in other studies. The DME sub-mechanism from Zhao et al. [37] was complemented with other reactions presented in Burke et al. [46] and Curran's kinetics model [27], which were not included in Zhao's mechanism [37].

DME reacts with several radicals to form CH₃OCH₂ through the abstraction of an H atom. Burke et al. [46] found that Zhao's reaction mechanism did not include the H-abstraction reaction from DME by CH₃O₂ radicals, which may be the reason for the high rates reported by Zhao et al. [37]. Rates for the reaction of DME with HO₂ were adopted from the quantum chemical calculations performed by Mendes et al., which are the same implemented in the chemical kinetic model proposed by Burke et al., while the rate coefficient expression for the reaction of DME with methylperoxyl radicals was estimated based on the calculations done by Carstensen and Dean [103]. CH₃OCH₂, on the other hand, reacts with O₂ at temperatures below 800 K [103]. The path leading to the formation of CH₂O and CH₃ from CH₃OCH₂ decomposition is only significant at very high temperature, according to Curran et al. [27]. The pre-exponential factor of Zhao's reaction rates for the dissociation of CH₃OCH₂ was decreased by a factor of 2, which is in accordance with the expression obtained by Li et al. [104] from their direct ab initio and density-functional theory dynamics study. The resulting rates are similar to the presented rates by Burke et al. for the pressure range of interest in this study. The pressure dependent rates for the oxidation of CH₃OCH₂ to CH₃CH₂OO were adopted from the studies of Burke et al. [46]. These are in accordance with the temperature independent expression proposed by Curran et al., at low temperatures, while higher discrepancies were observed with increasing temperature. CH₃OCH₂OO, a product of CH₃OCH₂ oxidation, rearranges through a H-shift to CH₂OCH₂OOH.

The subsequent reaction paths of $\text{CH}_2\text{OCH}_2\text{OOH}$ show a high dependence on the gas temperature, dissociating at intermediate temperatures and reacting with O_2 at lower ones [27,34]. The rate coefficients of $\text{CH}_3\text{OCH}_2\text{OO}$ isomerization reaction to $\text{CH}_2\text{OCH}_2\text{OOH}$ as well as the dissociation reaction of the latter species into one OH radical and two CH_2O molecules and the O_2 addition reaction to $\text{CH}_2\text{OCH}_2\text{OOH}$ presented in the mechanisms of Zhao et al. are the same as the rate expressions presented by Curran et al. in his analysis with regard to the low temperature chemistry of DME [27]. Rate expressions of both reactions comprising $\text{CH}_2\text{OCH}_2\text{OOH}$ were found to be too fast compared to the pressure dependence data from the study by Burke et al. Therefore, reactions comprising the dissociation of $\text{CH}_2\text{OCH}_2\text{OOH}$ into CH_2O and OH as well as the formation of $\text{OOCH}_2\text{OCH}_2\text{OOH}$ were modified by lowering their pre-exponential factors by a factor of 2.5 and 2, respectively. The pre-exponential factor of the $\text{CH}_3\text{OCH}_2\text{OO}$ H-shift reaction to $\text{CH}_2\text{OCH}_2\text{OOH}$ was also modified within its reported uncertainties.

5. Results and discussion

Experimental data of ignition delay times and species profiles measured in a rapid compression machine, a high-pressure shock tube and in a flow reactor for $\text{CH}_4/\text{DME}/\text{oxidizer}$ mixtures are compared in the following sections to simulation results. Simulations were performed implementing the polygeneration mechanism (PolyMech) and other reaction mechanisms from the literature, whose presentation is omitted since the experimental condition range presented in this work is out of their validation range.

5.1. Ignition delay times

Ignition delay times of CH_4/DME mixtures measured in a RCM for equivalence ratios of $\phi = 6, 7, 10,$ and 15 , $p_c = 10$ bar and at low and high temperatures (mixtures 3–6 and 7–10 in Table 1) are presented below. Shock-tube IDT data for mixtures at $\phi = 10$ (mixture 13) measured at 630–1500 K and 30 bar are also presented and compared to the predictions of the PolyMech (Section 4).

Measurements and simulations carried out for mixtures with $\phi = 1$ –2 are attached to this work as supplementary material, since these are not essential in the context of polygeneration but serve as additional validation targets for the mechanism.

For low-temperature measurements in the RCM, initial temperatures were increased to achieve higher temperatures at the end of compression while avoiding a possible ignition of the mixture during this process. Post-compression temperatures of $T_c = 660$ –740 K were obtained from experiments keeping the same initial pressure and mixture composition. Measurements at higher temperatures were not possible without ignition occurring already during compression, complicating the later data evaluation and calculation of the corresponding T_c . The oxidizer for the fuel mixtures in this section is a combination of argon and oxygen in air (ratio 79:21 Ar/O_2) as mentioned in Section 2.1.

Simulations of the experimental IDTs were carried out implementing the adiabatic-core model mentioned in Section 3. The results for mixtures 3–6 are displayed in Fig. 6. This figure shows IDTs as a function of the temperature reached at the end of compression for mixtures with equivalence ratios of $\phi = 6, 7, 10,$ and 15 . Two-stage ignition was observed for this set of experiments due to the presence of DME in the mixtures. In general, the predictions by PolyMech are in good agreement with the experimental data. PolyMech slightly under predicts the first-stage ignition delay times for $\phi = 7$ (Fig. 6b) at temperatures above 770 K while the main ignition is well predicted in the entire temperature range. A similar behavior can be seen for $\phi = 6$ (Fig. 6a) at temperatures above 700 K. Figure 6c shows a good agreement of the first stage of

ignition between predictions of PolyMech and the data measured in the RCM, while the main ignition is slightly under predicted by the model at temperatures around 715 K. The two-stage ignition behavior observed in the experiments was also reproduced in the simulations with PolyMech, showing that the developed mechanism is able to reproduce the partial oxidation process accurately.

In order to avoid ignition of the mixture during compression and to achieve higher post-compression temperatures, ignition delay time measurements in the RCM were carried out with mixtures having high contents of argon. The mixtures 7–10 (Table 1) present the same fuel/oxidizer ratio as the mixtures 3–6 with the difference that for the first case the argon/oxygen ratio was set to 95:5 Ar/O_2 instead of the conventional air ratio applied for the low-temperature measurements. This made it possible to reach post-compression temperatures of 870–1052 K. Comparison of simulations applying PolyMech with experimental data measured in the RCM for mixtures at $\phi = 6, 7, 10,$ and 15 are presented in Fig. 7.

For this case, the simulations were carried out implementing the multi-zone model instead of the adiabatic-core model since the reaction core remains adiabatic for a time span shorter than the measured IDTs, which makes the latter model inappropriate for the high temperature IDT computations.

For the high-temperature set of mixtures, only the main ignition was observed in the experiments while the simulations predict two-stage ignition. Species concentration profiles of DME and CH_4 for the conditions presented in Fig. 7 illustrate the two fuel components igniting separately from each other, corresponding to the first observable ignition to DME and the second one to methane. Figure 7 displays the results for the main ignition. It can be seen that predictions of PolyMech are generally in good agreement with experimental data. PolyMech slightly under predicts IDTs for mixtures at $\phi = 6$ and temperatures below 960 K (Fig. 7a) as well as for mixtures at $\phi = 7$ and temperatures between 960 and 1000 K (Fig. 7b). For higher equivalence ratios ($\phi > 10$, see Fig. 7c and d), the simulation results are in accordance with the measurements. In this set of mixtures, a slight temperature dependence was observed in experiments and simulations, resulting in almost flat curves especially for mixtures at $\phi > 10$.

Ignition delay times for fuel-rich CH_4/DME mixtures were also measured in a shock tube but this time at higher initial pressures than the pressures obtained after compression in the RCM and for temperatures up to 1500 K. Comparison of experimental data with the predictions of PolyMech for $\phi = 10$ mixtures and additive concentration of 10 mol% are presented in Fig. 8.

Figure 8 shows that the temperature dependence of the measurements is very well predicted by PolyMech. However, IDTs are over predicted by simulations for the entire temperature range. Similar deviations as presented in Fig. 8 were also observed for mixtures 11 and 12 with equivalence ratios of $\phi = 2$ (see supplementary material), indicating that the observed trends do not depend on the mixture composition.

Sensitivity analyses were carried out to determine the rate-limiting reaction steps as well as to identify the key reactions important for the kinetic description at the conditions studied in this work. Figure 9 shows OH global sensitivities for $\phi = 6$ and 10 at high and low temperatures. Figure 9a shows that at low temperatures, the rate-limiting reaction steps are dominated by DME decomposition and subsequently chain-branching reactions of DME's sub-products, explaining the importance of the DME sub-mechanism for the kinetic description and the prediction of the first ignition stages observed in Fig. 6. At low temperatures and an equivalence ratio of $\phi = 6$ (Fig. 9a), the most strongly inhibiting reaction is the H abstraction from DME by OH while the most promoting reaction is the H abstraction from methane. As the equivalence ratio increases, the sensitivities on DME sub-mechanism reactions are also increased, probably because of the lack of oxygen

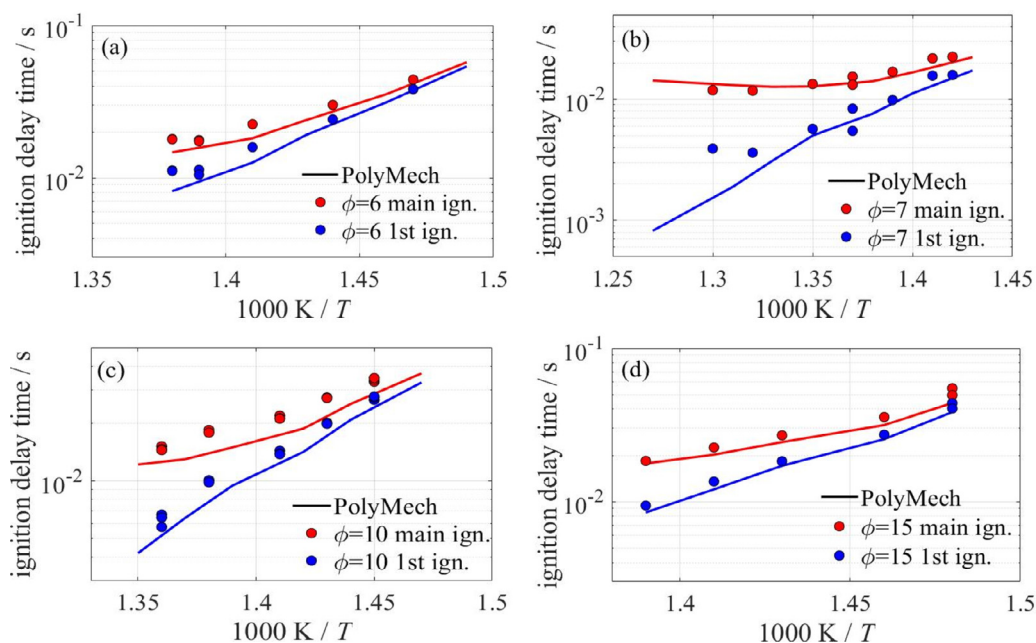


Fig. 6. Low-temperature ignition delay times measured in the RCM (symbols) and simulations based on PolyMech (straight lines) for (a) mixture 3, (b) mixture 4, (c) mixture 5, and (d) mixture 6. Blue lines represent the first-stage ignition and red lines the main ignition. (For interpretation of the references to color in this figure legend, the reader is referred to the web version of this article.)

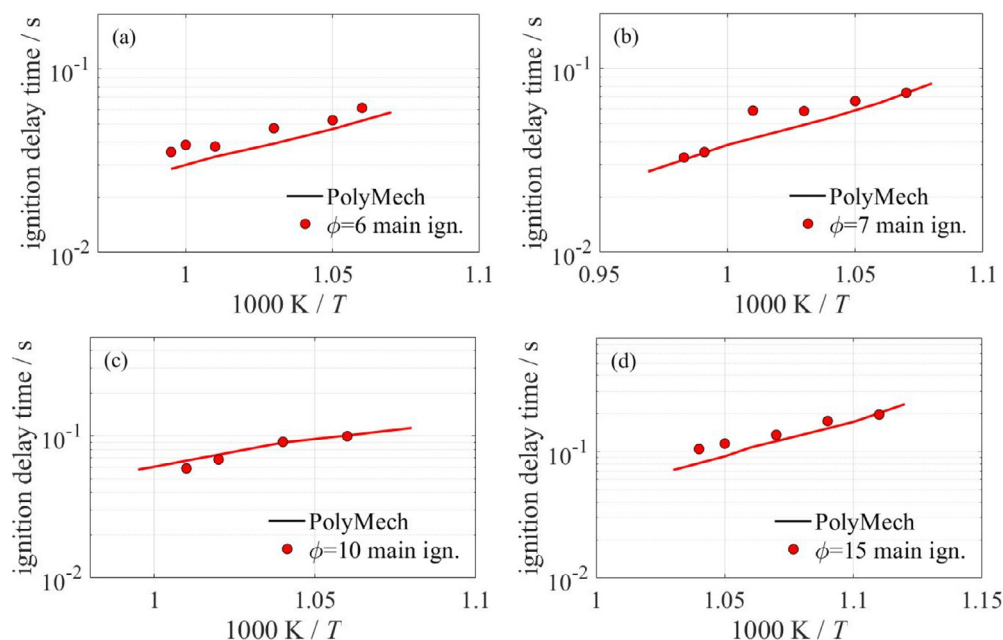


Fig. 7. High-temperature ignition delay times measured in the RCM (symbols) and simulations based on PolyMech (straight lines) for (a) mixture 7, (b) mixture 8, (c) mixture 9, and (d) mixture 10.

in the mixtures and the lowered temperatures reached in the gas-phase, causing lower methane conversion at higher equivalence ratios ($\phi > 10$).

Figure 9b displays OH global sensitivity analysis for high initial temperatures. It is shown that the sensitivity of H-abstraction reactions from CH_4 and DME by H, CH_3 , and HO_2 increased notably compared to the results in Fig. 9a. The recombination of methyl radicals to C_2H_6 is the most strongly inhibiting reaction for both equivalence ratios while the most promoting reactions are the H abstraction from DME as well as reactions comprising the dissociation of H_2O_2 and formation of CHO from CH_2O with CH_3 . Furthermore, an increase in the sensitivity of reactions involving H_2O_2 and HO_2 radicals can be seen in Fig. 9b.

5.2. Temporal variation of product concentrations

The temporal variation of the product composition of reacting CH_4/DME mixtures was measured in a RCEM for $\phi = 2, 6, \text{ and } 10$ (mixtures 14–16 in Table 1) at 714–738 K and 10 bar. In a flow reactor, species mole fractions were measured at the end of the reactor (Fig. 4) for mixtures at equivalence ratios of $\phi = 2, 10, \text{ and } 20$ (mixtures 17–22 in Table 1), 473–973 K and 6 bar. Shock-tube experimental data on species concentration after the ignition were also collected for mixtures at $\phi = 10$ (mixture 13) at 730–1310 K and 30 bar.

Comparisons between experimental data and simulations with PolyMech (Section 4) are presented below. Results for mixtures

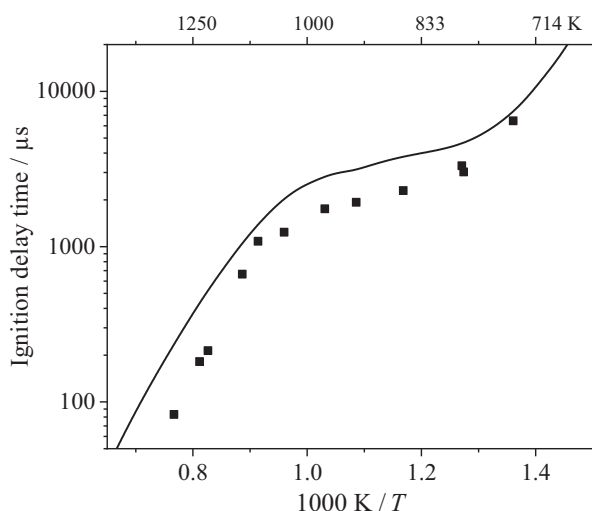


Fig. 8. Comparison of ignition delay times measured in a shock tube (symbols) and simulations with PolyMech (lines) for $\text{CH}_4/\text{DME}/\text{air}$ mixture at $\phi = 10$, 30 bar and with 10 mol% DME.

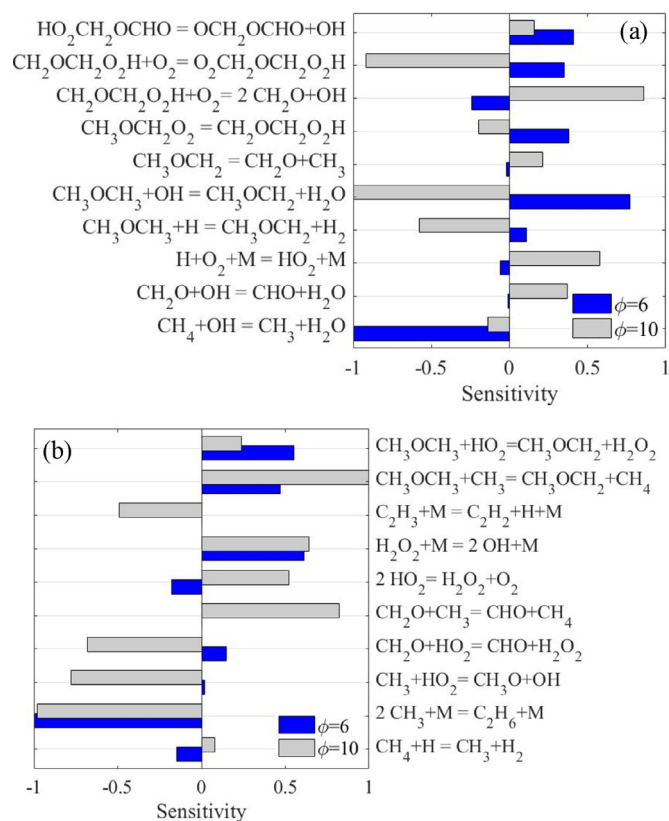


Fig. 9. Low and high temperatures global OH sensitivity analyses for mixtures at equivalence ratios of $\phi = 6$ and 10. (a) $T_c = 700\text{ K}$ (mixtures 3 and 5), (b) 950 K (mixtures 7 and 9).

with equivalence ratios of $\phi = 2$ and for mixtures 16 and 18 are attached to this work as supplementary material. Although very high pressures (above 30 bar) are not in the focus of our study, we compared also results of simulations using PolyMech with experimental data from the literature at $\phi = 20$ and 100 bar [12] (presented in the supplementary material).

The temporal consumption of reactants (CH_4 , DME, O_2) and the evolution of stable intermediates (CH_2O , C_2H_6 , C_2H_4 , C_2H_2 , CH_3OH)

and products (CO_2 , CO , H_2) during the ignition period were investigated in the RCEM. Simulations were performed applying the multi-zone model described in Section 3. It is important to note that some species are not completely frozen by the fast expansion of the piston but continue to react during this process. For this reason, simulations were carried out using the experimental volume curve which includes not only the compression but also the expansion phase, resulting in a detailed description of the experiments. Species mole fractions at the end of the expansion phase for each τ_{hold} were taken, as it was done for the experiments in order to avoid discrepancies between both of them in respect of further reactions of some species.

Figure 10 shows the remaining fraction of methane, DME, and oxygen plotted against the reaction time. A small initial increase in methane (values exceeding 100%) was observed in experiments for mixtures 15 and 16. A possible reason for this is the formation of CH_4 from DME at the first stages of reaction combined with the measurement uncertainties. This effect was also observed in simulations but in a smaller proportion, predicting an increase of less than 0.5% in the remaining fraction of methane. DME rapidly decreases at the initial steps of reaction while methane remains constant, explaining the strong dependence of ignition delay times on the DME sub-mechanism as observed in Fig. 9.

In Fig. 10 (left), complete consumption of DME and oxygen is observed while 60% of the initial mole fraction of methane still remains in the gas mixture. DME reacts with O_2 enabling methane conversion through radical formation and increasing the temperature of the mixture. Simulations at $\phi = 10$ in Fig. 10 (right) show a slightly lower consumption of CH_4 compared to experimental data while oxygen and DME concentration time profiles were predicted quite well. No change in the remaining amount of methane is observed after 30 ms in both cases, possibly due to the low gas temperatures insufficient to dissociate methane thermally and the unavailability of oxygen. Methane conversion decreases considerably with the increase of ϕ , with only negligible conversion (2% and less) at $\phi > 15$.

Results concerning the formation of major products like CO , CO_2 , and H_2 as well as temporal concentration profiles of stable C_2 species are displayed in Figs. 11 and 12, respectively. Figure 11 shows the proportion of C atoms to the initial amount of C atoms in the fuel of CO and CO_2 as well as the mole fraction of H_2 as a function of time. The main product for the mixtures at equivalence ratios of $\phi = 6$ (left) and $\phi = 10$ (right) is CO followed by H_2 . The comparison of simulated and experimental species profiles shows an overall good agreement. PolyMech under predicts the amount of CO in both cases, with a difference that it is more pronounced for mixture 15 ($\phi = 6$) at times around 0.015 s. Mole fractions of H_2 are slightly over predicted by simulations for both mixtures. Higher discrepancies were found for mixture 16 after 30 ms of reaction. The concentration profiles of CO_2 shown in Fig. 11 are over predicted by PolyMech. CO_2 is produced shortly after CO , reaching quickly constant values. This behavior is observed both in the simulations and the experiments. The amount of products observed in Fig. 11 decreases with increasing equivalence ratio. A possible explanation for this behavior is the strong decrease of methane conversion between $\phi = 6$ and $\phi = 10$ observed in Fig. 10 (the conversion of DME is nearly the same for both equivalence ratios), influencing the amount of C-atoms available for products.

Figure 12 displays the formation of C_2H_4 and C_2H_6 in C-atom proportions as a function of reaction time. The production of C_2H_4 is slightly over predicted for mixture 15 (Fig. 12 left) shortly after ignition, whereas the deviation rises with increasing time. For mixture 16, the ethylene concentration profile is predicted well. Simulations of ethane are in good agreement with the measurements at $\phi = 6$ up to 30 ms. At longer reaction times, the yield is slightly

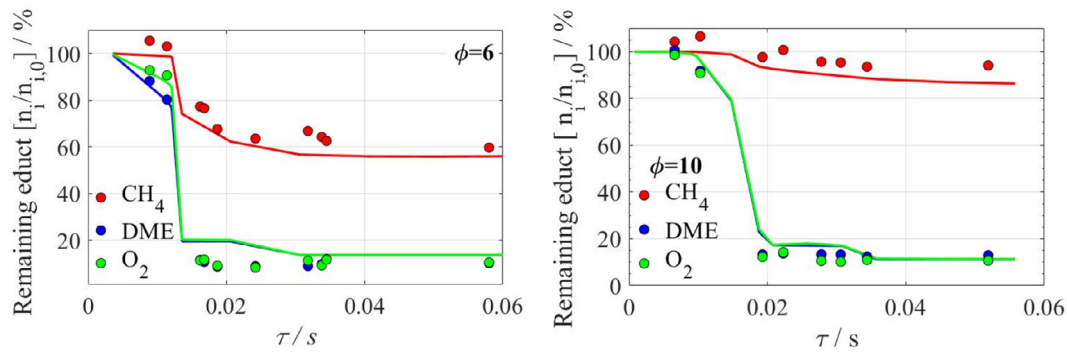


Fig. 10. Comparison of reactant's temporal consumption profiles for mixture 15 (left) and 16 (right) measured in an RCEM (symbols) and simulations (lines).

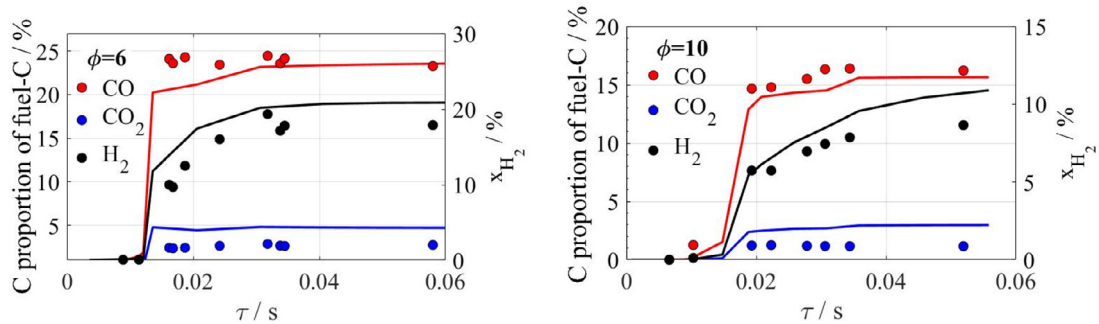


Fig. 11. Comparison of the CO, CO₂ and H₂ species profiles as a function of reaction time for mixture 15 (left) and 16 (right) measured in a RCEM (symbols) and simulations (lines).

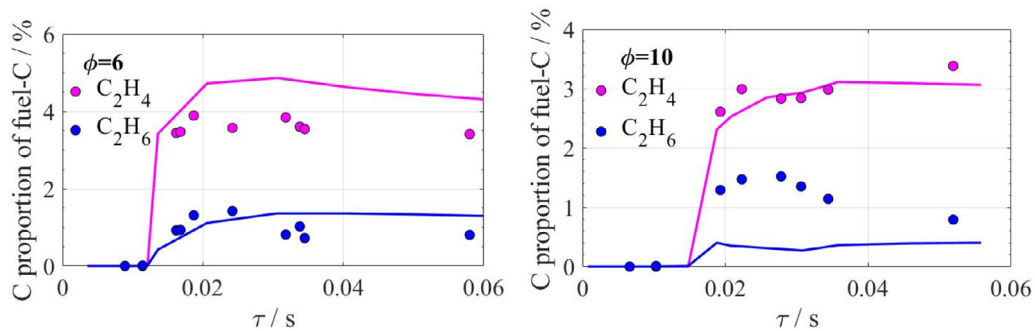


Fig. 12. Comparison of C₂ species formation time profiles for mixture 15 (left) and 16 (right) measured in an RCEM (symbols) and simulations (lines).

over predicted by the model. Experimental data of ethane are under predicted by simulations for all reaction times at $\phi = 10$.

Figure 12 indicates that the amount of products does not change as much with varying equivalence ratio, as it was observed for CO, CO₂, and H₂ in Fig. 11. Unsaturated C₂ species are mostly formed by a sequential H abstraction from C₂H₆ to produce C₂H₂. Methyl recombination to ethane is a primary termination reaction and is the major sink for CH₃ radicals (Fig. 13), which are formed either from CH₄ or DME and can be oxidized to formaldehyde, subsequently producing CO, or recombine to ethane. The path followed by these radicals is strongly influenced by the lack of oxygen in the mixtures, which is the reason why the second path prevails over the first one for mixtures at extremely high equivalence ratios as can be seen in Fig. 13. Ethane reacts to C₂H₄; ethylene, on the other hand, reacts to more than 90% to form acetylene while the other 10% are consumed to produce propene. The subsequent reactions of C₂H₂ are very complex. When formed, propyne and allyl will produce C₃H₃ at high temperatures, which mostly recombines and goes on to form benzene (main soot precursor).

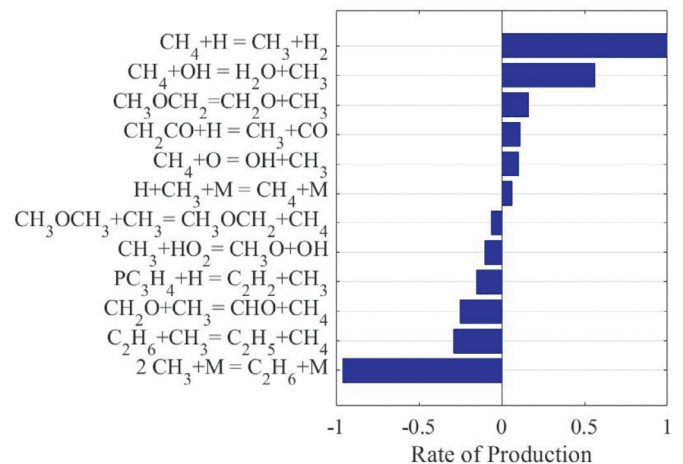


Fig. 13. Rate of production analysis on CH₃ for mixtures with equivalence ratios of $\phi = 6$.

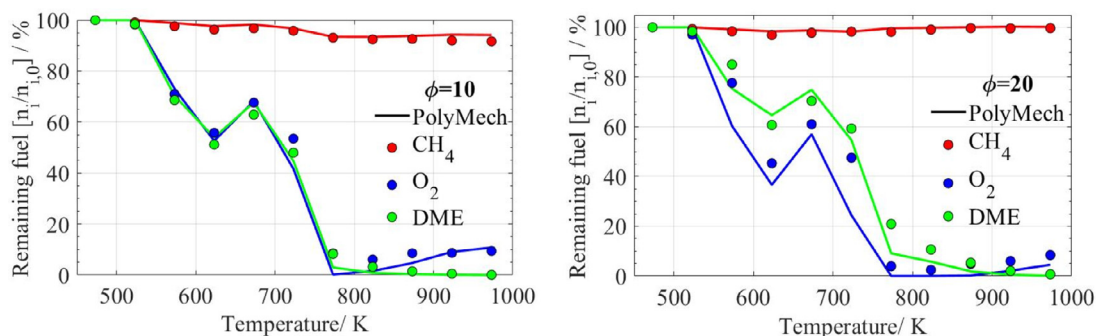


Fig. 14. Remaining fractions of reactants as a function of temperature for mixtures 20 (left) and 22 (right).

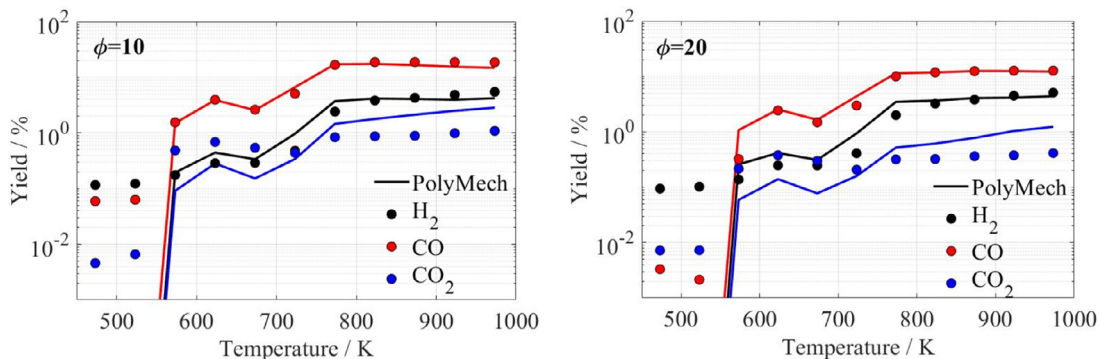


Fig. 15. Yields of CO, CO₂ and H₂ as a function of temperature for mixtures 20 (left) and 22 (right).

The decrease of the reactants and the formation of stable products as a function of temperature was investigated in the plug-flow reactor. In this case, gas mixture compositions at the end of the reactor were computed implementing the plug-flow simulation model mentioned in Section 3 and compared to experimental data.

Figure 14 shows the remaining fractions of CH₄, O₂ and DME as a function of temperature and equivalence ratio. The first consumption of the fuel takes place at temperatures higher than 523 K. This is shown by the decreasing fuel fraction of DME and CH₄ as well as by the consumption of O₂. DME decreases much faster than CH₄, which is caused by the higher reactivity of DME, as already shown in Fig. 10 for the species time profile measurements in the RCEM. Even at the highest investigated temperature of 973 K and $\phi = 10$, more than 90% of the CH₄ remains in the mixture, whereas DME is completely consumed at temperatures above 823 K. With increasing equivalence ratio, the fraction of remaining CH₄ also increases, reaching values higher than 100% at $\phi = 20$ and $T > 823$ K (mixture 22). This effect is caused by methane formation under these conditions. The trends and absolute values of the remaining fraction of methane and DME are predicted very well by the model, including the observed NTC region in the 623–773 K range. The remaining amount of O₂ is also in good agreement with the model predictions up to 773 K. At higher temperatures, higher O₂ consumption was observed for the mixtures with 5% DME (see supplementary materials) in the experiments. These deviations become smaller with increasing temperatures.

Yields of major products (CO, CO₂ and H₂) as well as higher hydrocarbons (C₂ and C₃ species) as a function of temperature and equivalence ratio are presented in Figs. 15 and 16. Figure 15 shows that CO is the main product in all experiments and that the yields of CO and CO₂ decrease with increasing ϕ from nearly 19% and 1% at $\phi = 10$ to 13% and less than 0.5% at $\phi = 20$ for CO and CO₂, respectively. The reason for this behavior is the lack of oxygen,

decreasing the reactivity of the mixtures. The lower conversion of methane and gas temperatures obtained at higher equivalence ratios are also a consequence of the low oxygen concentration. For H₂, on the other hand, yields nearly remain constant from $\phi = 10$ (5.5%) to 20 (5.1%). This suggests that most H₂ is formed by oxidation of DME, as DME is fully oxidized at temperatures higher than 823 K (Fig. 14). Additionally, the yields rise with increasing DME amount, whereas this effect is much more pronounced at $\phi \geq 10$, compared to $\phi = 2$ (see supplementary material).

In general, good agreement between simulations and experiments is found, especially regarding the trends of the product yields. Only for CO₂, the model predicts much higher yields in comparison to the experiments. This observation is similar to that in case of the RCEM experiments. Also, for H₂, the model slightly under predicts the yields in the 573–773 K range. The experimental data at 473–523 K can be neglected as they arise from the fluctuating background in the spectra of the TOF-MS.

C₂ and C₃ species are formed at temperatures higher than 723 K. The maximum yields of C₂H₄ were found at $\phi = 2$ (see supplementary material). The yields of C₂H₆, C₃H₆, and C₃H₈ show a local maximum at $\phi = 10$ within the investigated parameter range. Except for C₂H₄ at $\phi \geq 10$, the yields of these hydrocarbons decrease with increasing DME amount. Additionally, it can be noticed that the unsaturated hydrocarbons C₂H₄ and C₃H₆ are formed by H abstraction from C₂H₆ and C₃H₈ at higher temperatures, as the yields of the alkanes are exceeded by the alkene ones. As the temperatures are relatively low, no formation of C₂H₂ was observed. With respect to the simulations, an overall good agreement of the experimental and simulated data is found. For C₂H₄ and C₃H₆, the model under predicts the experimental data.

Species concentrations of several hydrocarbons including benzene, were measured after the ignition in a shock tube. The shock tube data were simulated for mixture 13 ($\phi = 10$) at 30 bar and 800 K (Fig. 17).

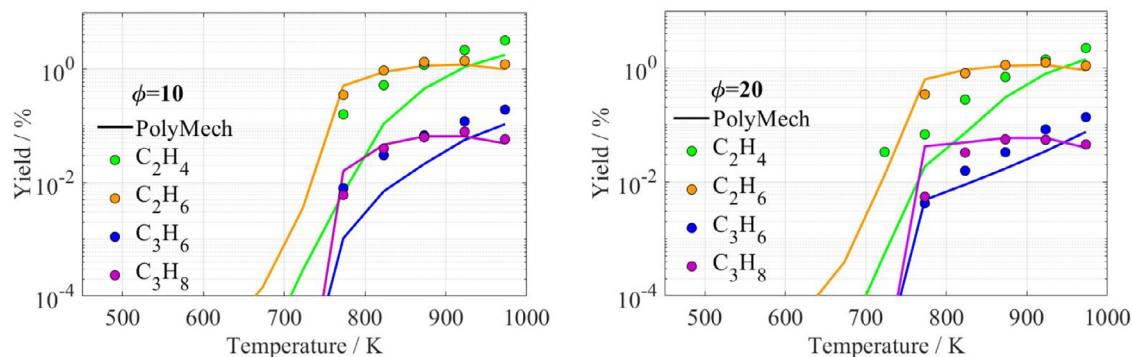


Fig. 16. Yields of C_2H_4 , C_2H_6 , C_3H_6 and C_3H_8 as a function of temperature for mixtures 20 (left) and 22 (right).

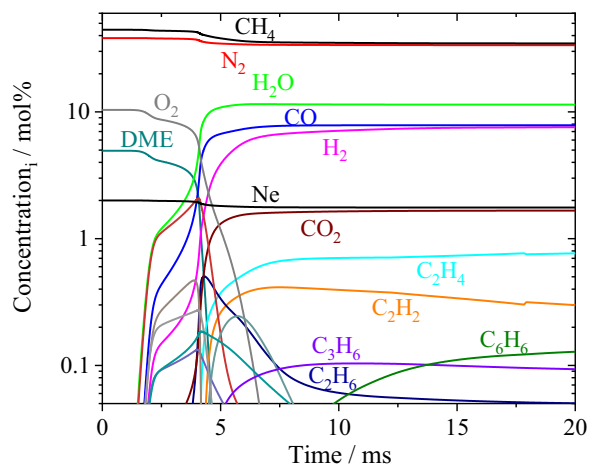


Fig. 17. Simulation of time dependent species profiles for shock tube conditions mixture 13 ($\phi = 10$) at 800 K and 30 bar.

The results in Fig. 17 show that the main reaction products at these conditions are H_2 , CO , H_2O , CO_2 , C_2H_4 , C_2H_2 , C_3H_6 , C_2H_6 , and C_6H_6 . The mole fractions of most species (except H_2 , C_2H_6 , and C_6H_6) reach nearly constant values about 2 ms after ignition while a temperature decrease is observable after the measurement time of 12 ms. The gas temperature decrease due to rarefaction waves is caused by the high heat capacity of the mixture that is not sufficient to stop radical reactions so that the benzene concentration steadily increases over time while the ethane concentration decreases. These radical reactions are stopped by the strong temperature decrease during sampling in the evacuated 50 ml vessel. In order to compare simulation results with the experimental data measured in a shock tube (Fig. 18), an average reaction time of 15 ms was assumed.

Figure 18 shows the results of the product measurements and simulations with PolyMech as a function of the initial temperatures. The product yields of the species displayed in Fig. 18, with the exception of benzene, show low dependence on the initial temperature. This is predicted well by the simulations. The absolute concentrations of C_2H_2 and CO are in good agreement with the simulations whereas for benzene much higher concentrations are predicted due to the lack of reactions in the mechanism describing the consumption of benzene. Benzene is considered to be a soot precursor and its further reactions lead to the formation of PAHs [105]. In this case, no further aromatic species or soot were detected during experiments. Although, it was not possible to measure benzene in the RCM and no benzene was detected in the flow

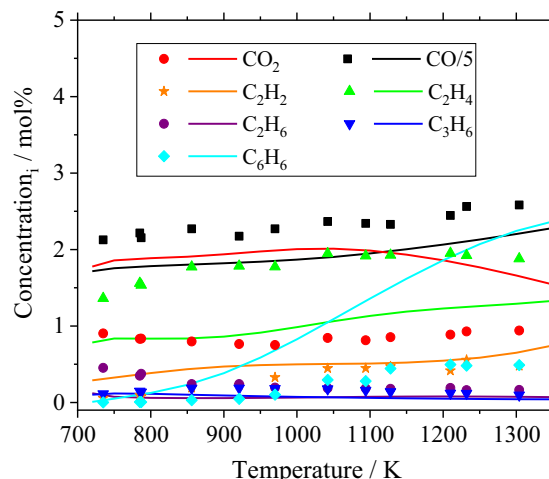


Fig. 18. Measured (shock tube, symbols) and simulated (straight lines) product mole fractions after ignition of $CH_4/DME/air$ mixture (mixture 13) at $\phi = 10$ and 30 bar.

reactor experiments, a carbon balance of all measured species in the RCM and the flow reactor does not suggest the presence of benzene or any other larger hydrocarbon molecule.

6. Conclusions

In this work, the oxidation of CH_4/DME mixtures under extremely fuel-rich conditions was investigated by measuring ignition delay times (IDTs) in a rapid compression machine (RCM) and in a shock tube as well as quasi-time resolved histories of stable species during the reaction in a rapid compression–expansion machine (RCM), a shock tube, and a flow reactor. The measurements cover an extended range of equivalence ratios ($\phi = 1–20$) to provide data that are of special interest for partial oxidation and polygeneration processes. The variation of product concentrations as a function of reaction time revealed syngas (CO and H_2) as a main product of the reaction of the studied mixtures; promising yields of valuable species like C_2H_4 and C_2H_2 were also observed.

Even though the formation of soot and PAHs is reported to be enhanced at low temperatures, none of these were observed in the experiments presented in this study, probably because of the presence of DME in the fuel mixtures. Small concentrations of benzene (considered as a soot precursor) were detected in shock tube experiments, showing a composition increase of the species with increasing temperatures above 1000 K. These high initial tempera-

tures could not be achieved in the RCM and flow reactor measurements.

A reaction mechanism (PolyMech) was developed with a special focus on the description of the ultra-rich reaction conditions important for polygeneration processes, since most of the chemical kinetics models found in the literature are validated only for the conventional combustion regime ($\phi = 0.5\text{--}2$). The PolyMech is based on existing mechanisms describing the oxidation and pyrolysis of methane as well as the reaction of DME, which was included in the fuel mixture as auto-ignition and reaction promoter. Sensitivities and reaction pathways analyses were carried out at different conditions in order to identify the rate-limiting reactions at the conditions covered in this study. It was found that at low temperatures, the sub-mechanism of DME plays an important role on the kinetics of the mixtures, as it provides radicals and increases the gas temperature promoting the further reaction of methane. At low temperatures, a two stage ignition was observed in experiments as well as in simulations. At higher temperatures, only one main ignition was observed; reaction analyses on these conditions showed an increase in the sensitivity of reactions including CH_2O and hydrogen sub-mechanisms.

With increasing equivalence ratios, a notoriously decrease of the methane conversion was observed, while DME and oxygen were completely consumed in all cases. An influence of the decreasing methane conversion was also observed in the formation of some species like C_2H_4 and C_2H_6 , which displayed smaller concentrations in the mixtures at higher equivalence ratios. An increase in the sensitivities of reactions including radicals like H and CH_3 with rising equivalence ratios was also observed. This was expected due to the lack of oxygen present in the initial mixtures at these conditions.

In order to improve the simulation predictions of experimental data in a wide range of conditions, rates of some limiting reactions were modified within their uncertainties as described in the Section 4 of this study. The identification of these reactions was carried out by applying sensitivity analyses at different temperatures and mixture compositions. The presented polygeneration mechanism (PolyMech) is shown to predict the measured ignition delay times and species concentration variations very well. But, it has to be noticed that further reactions describing the formation and reaction of benzene should be included in order to obtain better predictions of C_2 species profiles. Consequently, the PolyMech is a valuable tool for describing reactions in the ultra-rich regime, which is relevant for several future combustion applications.

Declaration of Competing Interest

The authors declare that they have no known competing financial interests or personal relationships that could have appeared to influence the work reported in this paper.

Acknowledgements

Financial support of this work by the German Research Foundation within the framework of the DFG research unit FOR 1993 'Multi-functional conversion of chemical species and energy' (projects MA 1205/20, SCHI 647/3, SCHU 1369/19 and KA 3871/1-2) is gratefully acknowledged.

Supplementary materials

Supplementary material associated with this article can be found, in the online version, at doi:[10.1016/j.combustflame.2019.09.036](https://doi.org/10.1016/j.combustflame.2019.09.036).

References

- [1] G. Chicco, P. Mancarella, Distributed multi-generation: a comprehensive view, *Renew. Sustain. Energy Rev.* 13 (2009) 535–551.
- [2] B. Atakan, Gas turbines for polygeneration? a thermodynamic investigation of a fuel rich gas turbine cycle, *Int. J. Thermodyn.* 14 (2011) 185–192.
- [3] R. Hegner, B. Atakan, A polygeneration process concept for HCCI-engines – Modeling product gas purification and exergy losses, *Int. J. Hydrog. Energy* 42 (2017) 1287–1297.
- [4] H. Gossler, O. Deutschmann, Numerical optimization and reaction flow analysis of syngas production via partial oxidation of natural gas in internal combustion engines, *Int. J. Hydrog. Energy* 40 (2015) 11046–11058.
- [5] K.J. Hughes, T. Turányi, A.R. Clague, M.J. Pilling, Development and testing of a comprehensive chemical mechanism for the oxidation of methane, *Int. J. Chem. Kinet.* 33 (2001) 513–538.
- [6] E.L. Petersen, D.F. Davidson, R.K. Hanson, Kinetics modeling of shock-induced ignition in low-dilution CH_4/O_2 mixtures at high pressures and intermediate temperatures, *Combust. Flame* 117 (1999) 272–290.
- [7] L. Brett, J. Macnamara, P. Musch, J.M. Simmie, Simulation of methane autoignition in a rapid compression machine with creviced pistons, *Combust. Flame* 124 (2001) 326–329.
- [8] S. Gersen, N.B. Anikin, A.V. Mokhov, H.B. Levinsky, Ignition properties of methane/hydrogen mixtures in a rapid compression machine, *Int. J. Hydrog. Energy* 33 (2008) 1957–1964.
- [9] V. Zhukov, V. Sechenov, A.Y. Starikovskii, Spontaneous ignition of methane-air mixtures in a wide range of pressures, combustion, *Explos. Shock Waves* 39 (2003) 487–495.
- [10] T.A. Ano, F.L. Dryer, Effect of dimethyl ether, NOx, and ethane on CH_4 oxidation: High pressure, intermediate-temperature experiments and modeling, *Symp. (Int.) Combust.* 27 (1998) 397–404.
- [11] P. Glarborg, L.L.B. Bentzen, Chemical effects of a high CO_2 concentration in oxy-fuel combustion of methane, *Energy Fuels* 22 (2008) 291–296.
- [12] H. Hashemi, J.M. Christensen, S. Gersen, H. Levinsky, S.J. Klippenstein, P. Glarborg, High-pressure oxidation of methane, *Combust. Flame* 172 (2016) 349–364.
- [13] C.L. Rasmussen, J. Hansen, P. Marshall, P. Glarborg, Experimental measurements and kinetic modeling of $\text{CO}/\text{H}_2/\text{O}_2/\text{NO}_x$ conversion at high pressure, *Int. J. Chem. Kinet.* 40 (2008) 454–480.
- [14] P. Dagaut, J.-C. Boettner, M. Cathonnet, Methane oxidation: Experimental and kinetic modeling study, *Combust. Sci. Technol.* 77 (1991) 127–148.
- [15] D. Healy, H.J. Curran, J.M. Simmie, D.M. Kalitan, C.M. Zinner, A.B. Barrett, E.L. Petersen, G. Bourque, Methane/ethane/propane mixture oxidation at high pressures and at high, intermediate and low temperatures, *Combust. Flame* 155 (2008) 441–448.
- [16] F. Larkins, A.Z. Khan, Pyrolysis of methane to higher hydrocarbons: a thermodynamic study, *Aust. J. Chem.* 42 (1989) 1655–1670.
- [17] O. Olsvik, O.A. Rokstad, A. Holmen, Pyrolysis of methane in the presence of hydrogen, *Chem. Eng. Technol.* 18 (1995) 349–358.
- [18] C. Keramiotis, G. Vourliotakis, G. Skevis, M.A. Founti, C. Esarte, N.E. Sánchez, A. Millera, R. Bilbao, M.U. Alzueta, Experimental and computational study of methane mixtures pyrolysis in a flow reactor under atmospheric pressure, *Energy* 43 (2012) 103–110.
- [19] H.-S. Kang, D.H. Lee, K.-T. Kim, S. Jo, S. Pyun, Y.-H. Song, S. Yu, Methane to acetylene conversion by employing cost-effective low-temperature arc, *Fuel Process. Technol.* 148 (2016) 209–216.
- [20] N. Muradov, F. Smith, C. Huang, A. T-Raissi, Autothermal catalytic pyrolysis of methane as a new route to hydrogen production with reduced CO_2 emissions, *Catal. Today* 116 (2006) 281–288.
- [21] T.A. Semelsberger, R.L. Borup, H.L. Greene, Dimethyl ether (DME) as an alternative fuel, *J. Power Sources* 156 (2006) 497–511.
- [22] P. Dagaut, J.C. Boettner, M. Cathonnet, Chemical kinetic study of dimethylether oxidation in a jet stirred reactor from 1 to 10 ATM: experiments and kinetic modeling, *Symp. (Int.) Combust.* (1996), doi:[10.1016/S0082-0784\(96\)80269-4](https://doi.org/10.1016/S0082-0784(96)80269-4).
- [23] S.L. Fischer, F.L. Dryer, H.J. Curran, The reaction kinetics of dimethyl ether. I: high-temperature pyrolysis and oxidation in flow reactors, *Int. J. Chem. Kinet.* 32 (2000) 713–740.
- [24] E.W. Kaiser, T.J. Wallington, M.D. Hurley, J. Platz, H.J. Curran, W.J. Pitz, C.K. Westbrook, Experimental and modeling study of premixed atmospheric-pressure dimethyl ether–air flames, *J. Phys. Chem. A* 104 (2000) 8194–8206.
- [25] H.J. Curran, W.J. Pitz, C.K. Westbrook, P. Dagaut, J.-C. Boettner, M. Cathonnet, A wide range modeling study of dimethyl ether oxidation, *Int. J. Chem. Kinet.* 30 (1998) 229–241.
- [26] M.C. Lee, S.B. Seo, J.H. Chung, Y.J. Joo, D.H. Ahn, Industrial gas turbine combustion performance test of DME to use as an alternative fuel for power generation, *Fuel* 88 (2009) 657–662.
- [27] H.J. Curran, S.L. Fischer, F.L. Dryer, The reaction kinetics of dimethyl ether. II: low-temperature oxidation in flow reactors, *Int. J. Chem. Kinet.* 32 (2000) 741–759.
- [28] P. Dagaut, C. Daly, J.M. Simmie, M. Cathonnet, The oxidation and ignition of dimethylether from low to high temperature (500–1600K): Experiments and kinetic modeling, *Symp. (Int.) Combust.* 27 (1) (1998) 361–369.
- [29] A. McIlroy, T.D. Hain, H.A. Michelsen, T.A. Cool, A laser and molecular beam mass spectrometer study of low-pressure dimethyl ether flames, *Proc. Combust. Inst.* 28 (2) (2000) 1647–1653.

- [30] U. Pfahl, K. Fieweger, G. Adomeit, Self-ignition of diesel-relevant hydrocarbon-air mixtures under engine conditions, *Symp. (Int.) Combust.* 26 (1) (1996) 781–789.
- [31] X. Zheng, T. Lu, C.K. Law, C. Westbrook, H. Curran, Experimental and computational study of nonpremixed ignition of dimethyl ether in counterflow, *Proc. Combust. Inst.* 30 (2005) 1101–1109.
- [32] C.A. Daly, J.M. Simmie, J. Würmel, N. Djeballi, C. Paillard, Burning velocities of dimethyl ether and air, *Combust. Flame* 125 (2001) 1329–1340.
- [33] X. Qin, Y. Ju, Measurements of burning velocities of dimethyl ether and air premixed flames at elevated pressures, *Proc. Combust. Inst.* 30 (2005) 233–240.
- [34] A. Andersen, E.A. Carter, A hybrid density functional theory study of the low-temperature dimethyl ether combustion pathways. I: chain-propagation, *Israel J. Chem.* 42 (2002) 245–260.
- [35] A. Andersen, E.A. Carter, Hybrid density functional theory predictions of low-temperature dimethyl ether combustion pathways. II. Chain-branching energetics and possible role of the Criegee intermediate, *J. Phys. Chem. A* 107 (2003) 9463–9478.
- [36] J.J. Nash, J.S. Francisco, Unimolecular decomposition pathways of dimethyl ether: an ab initio study, *J. Phys. Chem. A* 102 (1998) 236–241.
- [37] Z. Zhao, M. Chaos, A. Kazakov, F.L. Dryer, Thermal decomposition reaction and a comprehensive kinetic model of dimethyl ether, *Int. J. Chem. Kinet.* 40 (2008) 1–18.
- [38] R. Sivaramakrishnan, J.V. Michael, A.F. Wagner, R. Dawes, A.W. Jasper, L.B. Harding, Y. Georgievskii, S.J. Klippenstein, Roaming radicals in the thermal decomposition of dimethyl ether: experiment and theory, *Combust. Flame* 158 (2011) 618–632.
- [39] Y. Hidaka, K. Sato, M. Yamane, High-temperature pyrolysis of dimethyl ether in shock waves, *Combust. Flame* 123 (2000) 1–22.
- [40] J. de Vries, W.B. Lowry, Z. Serinyel, H.J. Curran, E.L. Petersen, Laminar flame speed measurements of dimethyl ether in air at pressures up to 10atm, *Fuel* 90 (2011) 331–338.
- [41] T. Amano, F.L. Dryer, Effect of dimethyl ether, NO_x, and ethane on CH₄ oxidation: High pressure, intermediate-temperature experiments and modeling, *Symp. (Int.) Combust.* 27 (1) (1998) 397–404.
- [42] Z. Chen, X. Qin, Y. Ju, Z. Zhao, M. Chaos, F.L. Dryer, High temperature ignition and combustion enhancement by dimethyl ether addition to methane-air mixtures, *Proc. Combust. Inst.* 31 (2007) 1215–1222.
- [43] C. Tang, L. Wei, J. Zhang, X. Man, Z. Huang, Shock tube measurements and kinetic investigation on the ignition delay times of methane/dimethyl ether mixtures, *Energy Fuels* 26 (2012) 6720–6728.
- [44] W.B. Lowry, Z. Serinyel, M.C. Krejci, H.J. Curran, G. Bourque, E.L. Petersen, Effect of methane-dimethyl ether fuel blends on flame stability, laminar flame speed, and Markstein length, *Proc. Combust. Inst.* 33 (2011) 929–937.
- [45] S.S. Yoon, D.H. Anh, S.H. Chung, Synergistic effect of mixing dimethyl ether with methane, ethane, propane, and ethylene fuels on polycyclic aromatic hydrocarbon and soot formation, *Combust. Flame* 154 (2008) 368–377.
- [46] U. Burke, K.P. Somers, P. O'Toole, C.M. Zinner, N. Marquet, G. Bourque, E.L. Petersen, W.K. Metcalfe, Z. Serinyel, H.J. Curran, An ignition delay and kinetic modeling study of methane, dimethyl ether, and their mixtures at high pressures, *Combust. Flame* 162 (2015) 315–330.
- [47] H. Hashemi, J.M. Christensen, P. Glarborg, High-pressure pyrolysis and oxidation of DME and DME/CH₄, *Combust. Flame* (2019) 80–92, doi:10.1016/j.combustflame.2019.03.028.
- [48] Y. Hidaka, K. Sato, Y. Henmi, H. Tanaka, K. Inami, Shock-tube and modeling study of methane pyrolysis and oxidation, *Combust. Flame* 118 (1999) 340–358.
- [49] C.I. Heghes, C1–C4 hydrocarbon oxidation mechanism, Heidelberg University, Heidelberg, 2006.
- [50] M. Werler, L.R. Cancino, R. Schiessl, U. Maas, C. Schulz, M. Fikri, Ignition delay times of diethyl ether measured in a high-pressure shock tube and a rapid compression machine, *Proc. Combust. Inst.* 35 (2015) 259–266.
- [51] G. Mittal, C.-J. Sung, A rapid compression machine for chemical kinetics studies at elevated pressures and temperatures, *Combust. Sci. Technol.* 179 (2007) 497–530.
- [52] X. He, S.M. Walton, B.T. Zigler, M.S. Wooldridge, A. Atreya, Experimental investigation of the intermediates of isoctane during ignition, *Int. J. Chem. Kinet.* 39 (2007) 498–517.
- [53] D. Lee, S. Hochgreb, Rapid compression machines: Heat transfer and suppression of corner vortex, *Combust. Flame* 114 (1998) 531–545.
- [54] J. Würmel, J.M. Simmie, CFD studies of a twin-piston rapid compression machine, *Combust. Flame* 141 (2005) 417–430.
- [55] M. Werler, Untersuchungen der niederer-temperatur-oxidation von kohlenwasserstoffen in einer schnellen kompressions-expansions-maschine, Karlsruhe Institut für Technologie (KIT), 2016.
- [56] H. Oertel, Stossrohre: theorie, praxis, anwendungen, mit einer einföhrung in die physik der gase, Shock Tubes, Springer-Verlag, Vienna, 1966.
- [57] H. Palmer, B.E. Knox, Contact surface tailoring in a chemical shock tube, *ARS J.* 31 (1961) 826–828.
- [58] D. Kaczmarek, B. Atakan, T. Kasper, Plug-Flow reactor study of the partial oxidation of methane and natural gas at ultra-rich conditions, *Combust. Sci. Technol.* (2019) 1–14, doi:10.1080/00102202.2019.1577829.
- [59] F. Sen, B. Shu, T. Kasper, J. Herzler, O. Welz, M. Fikri, B. Atakan, C. Schulz, Shock-tube and plug-flow reactor study of the oxidation of fuel-rich CH₄/O₂ mixtures enhanced with additives, *Combust. Flame* 169 (2016) 307–320.
- [60] M. Werler, R. Schießl, U. Maas, A rapid compression expansion machine (RCEM) for measuring species histories, *Proceedings of 26th International Colloquium on the Dynamics of Explosions and Reactive Systems, ICEDERS*, Boston, USA (2017).
- [61] J. Herzler, Y. Sakai, M. Fikri, C. Schulz, Shock-tube study of the ignition and product formation of fuel-rich CH₄/air and CH₄/additive/air mixtures at high pressure, *Proc. Combust. Inst.* 37 (2019) 5705–5713.
- [62] D. Kaczmarek, B. Atakan, T. Kasper, Investigation of the partial oxidation of methane/n-heptane-mixtures and the interaction of methane and n-heptane under ultra-rich conditions, *Combust. Flame* 205 (2019) 345–357.
- [63] D.L. Baulch, C.T. Bowman, C.J. Cobos, R.A. Cox, T. Just, J.A. Kerr, M.J. Pilling, D. Stocker, J. Troe, W. Tsang, R.W. Walker, J. Warnatz, Evaluated kinetic data for combustion modeling: Supplement ii, *J. Phys. Chem. Ref. Data* 34 (2005) 757–1397.
- [64] A. Kéromnès, W.K. Metcalfe, K.A. Heufer, N. Donohoe, A.K. Das, C.-J. Sung, J. Herzler, C. Naumann, P. Griebel, O. Mathieu, M.C. Krejci, E.L. Petersen, W.J. Pitz, H.J. Curran, An experimental and detailed chemical kinetic modeling study of hydrogen and syngas mixture oxidation at elevated pressures, *Combust. Flame* 160 (2013) 995–1011.
- [65] W.G. Mallard, F. Westley, J. Herron, R.F. Hampson, D. Frizzell, NIST chemical kinetics database, National Institute of Standards and Technology, Gaithersburg, MD, 1998 version 2Q98.
- [66] C. Heghes, V. Karbach, J. Warnatz, Evaluation of new data for hydrocarbon kinetics, *Proceedings of the 2nd European Combustion Meeting, ECM*, Louvain-la-Neuve, Belgium (2005).
- [67] K. Hoyermann, F. Mauß, T. Zeuch, A detailed chemical reaction mechanism for the oxidation of hydrocarbons and its application to the analysis of benzene formation in fuel-rich premixed laminar acetylene and propene flames, *Phys. Chem. Chem. Phys.* 6 (2004) 3824–3835.
- [68] Y. Hidaka, H. Masaoka, H. Oshita, T. Nakamura, K. Tanaka, H. Kawano, Thermal decomposition of vinylacetylene in shock waves, *Int. J. Chem. Kinet.* 24 (1992) 871–885.
- [69] Y. Hidaka, T. Nakamura, A. Miyauchi, T. Shiraiishi, H. Kawano, Thermal decomposition of propyne and allene in shock waves, *Int. J. Chem. Kinet.* 21 (1989) 643–666.
- [70] N.M. Marinov, A detailed chemical kinetic model for high temperature ethanol oxidation, *Int. J. Chem. Kinet.* 31 (1999) 183–220.
- [71] M. Scott, R.W. Walker, Addition of toluene and ethylbenzene to mixtures of H₂ and O₂ at 773 K. Part I: kinetic measurements for h and HO₂ reactions with the additives and a data base for h abstraction by HO₂ from alkanes, aromatics and related compounds, *Combust. Flame* 129 (2002) 365–377.
- [72] C.-J. Chen, J.W. Bozzelli, Thermochemical property, pathway and kinetic analysis on the reactions of allylic isobutenyl radical with O₂: an elementary reaction mechanism for isobutene oxidation, *J. Phys. Chem. A* 104 (2000) 9715–9732.
- [73] R.R. Baldwin, P.N. Jones, R.W. Walker, Determination of the rate constant for $h_2 + CH_4 \rightarrow H_2 O_2 + CH_3$ at 443°C, *J. Chem. Soc. Faraday Trans. 2 Mol. Chem. Phys.* 84 (1988) 199–207.
- [74] N. Cohen, The use of transition-state theory to extrapolate rate coefficients for reactions of h atoms with alkanes, *Int. J. Chem. Kinet.* 23 (1991) 683–700.
- [75] J. Sutherland, M.C. Su, J. Michael, Rate constants for H+ CH₄, CH₃+ H₂, and CH₄ dissociation at high temperature, *Int. J. Chem. Kinet.* 33 (2001) 669–684.
- [76] W.K. Metcalfe, S.M. Burke, S.S. Ahmed, H.J. Curran, A hierarchical and comparative kinetic modeling study of C₁–C₂ hydrocarbon and oxygenated fuels, *Int. J. Chem. Kinet.* 45 (2013) 638–675.
- [77] R. Zhu, C. Lin, The CH₃+ HO₂ reaction: first-principles prediction of its rate constant and product branching probabilities, *J. Phys. Chem. A* 105 (2001) 6243–6248.
- [78] I.A.B. Reid, C. Robinson, D.B. Smith, Spontaneous ignition of methane: measurement and chemical model, *Symp. (Int.) Combust.* 20 (1985) 1833–1843.
- [79] K. Glänzer, M. Quack, J. Troe, A spectroscopic determination of the methyl radical recombination rate constant in shock waves, *Chem. Phys. Lett.* 39 (1976) 304–309.
- [80] H. Hippler, K. Luther, A.R. Ravishankara, J. Troe, High-Pressure effects in the recombination reaction CH₃+CH₃→C₂H₆, *Z. Phys. Chem.* (1984) 1.
- [81] I.R. Slagle, D. Gutman, J.W. Davies, M.J. Pilling, Study of the recombination reaction CH₃+CH₃→C₂H₆. 1. Experiment, *J. Phys. Chem.* 92 (1988) 2455–2462.
- [82] M.T. Macpherson, M.J. Pilling, M.J. Smith, Determination of the absorption cross section for methyl at 216.36nm and the absolute rate constant for methyl radical recombination over the temperature range 296–577K, *J. Phys. Chem.* 89 (1985) 2268–2274.
- [83] D. Walter, H.-H. Grotheer, J.W. Davies, M.J. Pilling, A.F. Wagner, Experimental and theoretical study of the recombination reaction CH₃+CH₃→C₂H₆, *Symp. (Int.) Combust.* 23 (1991) 107–114.
- [84] M.A. Blitz, N.J.B. Green, R.J. Shannon, M.J. Pilling, P.W. Seakins, C.M. Western, S.H. Robertson, Reanalysis of rate data for the reaction CH₃+CH₃→C₂H₆ using revised cross sections and a linearized second-order master equation, *J. Phys. Chem. A* 119 (2015) 7668–7682.
- [85] C. Oehlers, H.G. Wagner, H. Ziemer, F. Temps, S. Dobe, An investigation of the d/h addition–elimination and h atom abstraction channels in the reaction D+ H₂CO in the temperature range 296 K ≤ T ≤ 780K, *J. Phys. Chem. A* 104 (2000) 10500–10510.
- [86] J. Vandooren, L.O. de Guertechin, P. Van Tiggelen, Kinetics in a lean formaldehyde flame, *Combust. Flame* 64 (1986) 127–139.
- [87] A. Westenberg, N. DeHaas, Measurement of the rate constant for H+ H₂CO. Far. H₂+ HCO at 297–652. *Deg. K. J. Phys. Chem.* 76 (1972) 2213–2214.

- [88] E.A. Irdam, J.H. Kiefer, L.B. Harding, A.F. Wagner, The formaldehyde decomposition chain mechanism, *Int. J. Chem. Kinet.* 25 (1993) 285–303.
- [89] B. Eiteneer, C.-L. Yu, M. Goldenberg, M. Frenklach, Determination of rate coefficients for reactions of formaldehyde pyrolysis and oxidation in the gas phase, *J. Phys. Chem. A* 102 (1998) 5196–5205.
- [90] A.M. Held, K.C. Manthorne, P.D. Pacey, H.P. Reinholdt, Individual rate constants of methyl radical reactions in the pyrolysis of dimethyl ether, *Can. J. Chem.* 55 (1977) 4128–4134.
- [91] C. Anastasi, Reaction of methyl radicals with formaldehyde in the range $500 \leq T/K \leq 603$, *J. Chem. Soc. Faraday Trans. 1 Phys. Chem. Condens. Phases* 79 (1983) 749–753.
- [92] T.K. Choudhury, W. Sanders, M. Lin, A shock tube and modeling study of the methyl+ formaldehyde reaction at high temperatures, *J. Phys. Chem.* 93 (1989) 5143–5147.
- [93] J.A. Kerr, M.J. Parsonage, Evaluated kinetic data on gas phase hydrogen transfer reactions of methyl radicals, Butterworths, 1976.
- [94] J. Warnatz, Rate coefficients in the C/H/O system, combustion chemistry, Springer, 1984, pp. 197–360.
- [95] W. Tsang, R. Hampson, Chemical kinetic data base for combustion chemistry. Part I. Methane and related compounds, *J. Phys. Chem. Ref. Data* 15 (1986) 1087–1279.
- [96] J.M. Dyke, A.P. Groves, E.P.F. Lee, M.H. Zamanpour Niavaran, Study of the CH_3CHOH radical with ultraviolet photoelectron spectroscopy, *J. Phys. Chem. A* 101 (1997) 373–376.
- [97] Z. Hong, D. Davidson, E. Barbour, R. Hanson, A new shock tube study of the $\text{H} + \text{O}_2 \rightarrow \text{OH} + \text{o}$ reaction rate using tunable diode laser absorption of H_2O near $2.5 \mu\text{m}$, *Proc. Combust. Inst.* 33 (2011) 309–316.
- [98] R.W. Bates, D.M. Golden, R.K. Hanson, C.T. Bowman, Experimental study and modeling of the reaction $\text{H} + \text{O}_2 + \text{M} \rightarrow \text{HO}_2 + \text{M}$ ($\text{M} = \text{Ar}, \text{N}_2, \text{H}_2\text{O}$) at elevated pressures and temperatures between 1050 and 1250K, *Phys. Chem. Chem. Phys.* 3 (2001) 2337–2342.
- [99] R. Fernandes, K. Luther, J. Troe, V. Ushakov, Experimental and modelling study of the recombination reaction $\text{H} + \text{O}_2 (+ \text{M}) \rightarrow \text{H}_2\text{O}_2 (+ \text{M})$ between 300 and 900K, 1.5 and 950bar, and in the bath gases $\text{M} = \text{He}, \text{Ar},$ and N_2 , *Phys. Chem. Chem. Phys.* 10 (2008) 4313–4321.
- [100] J. Troe, The thermal dissociation/recombination reaction of hydrogen peroxide $\text{H}_2\text{O}_2(+\text{M}) \rightleftharpoons 2\text{OH}(+\text{M})$ III.: Analysis and representation of the temperature and pressure dependence over wide ranges, *Combust. Flame* 158 (2011) 594–601.
- [101] H. Hippler, J. Troe, J. Willner, Shock wave study of the reaction $\text{HO}_2 + \text{HO}_2 \rightarrow \text{H}_2\text{O}_2 + \text{O}_2$: confirmation of a rate constant minimum near 700K, *J. Chem. Phys.* 93 (1990) 1755–1760.
- [102] B.A. Ellingson, D.P. Theis, O. Tishchenko, J. Zheng, D.G. Truhlar, Reactions of hydrogen atom with hydrogen peroxide, *J. Phys. Chem. A* 111 (2007) 13554–13566.
- [103] H.-H. Carstensen, A.M. Dean, Rate constants for the abstraction reactions $\text{RO}_2 + \text{C}_2\text{H}_6$; $\text{R} = \text{H}, \text{CH}_3,$ and C_2H_5 , *Proc. Combust. Inst.* 30 (2005) 995–1003.
- [104] Q.S. Li, Y. Zhang, S. Zhang, Dual level direct ab initio and density-functional theory dynamics study on the unimolecular decomposition of CH_3OCH_2 radical, *J. Phys. Chem. A* 108 (2004) 2014–2019.
- [105] L. Cai, H. Pitsch, Optimized chemical mechanism for combustion of gasoline surrogate fuels, *Combust. Flame* 162 (2015) 1623–1637.
- [106] J.W. Sutherland, J.V. Michael, A.N. Pirraglia, F.L. Nesbitt, R.B. Klemm, Rate constant for the reaction of $\text{O} (3\text{P})$ with H_2 by the flash photolysis–shock tube and flash photolysis–resonance fluorescence techniques; $504 \text{ K} \leq T \leq 2495 \text{ K}$, *Symp. Int. Combust.* 21 (1988) 929–941.
- [107] D.A. Masten, R.K. Hanson, C.T. Bowman, Shock tube study of the reaction hydrogen atom+ oxygen. $\text{H} + \text{O}_2 \rightarrow \text{OH} + \text{O}$ using hydroxyl laser absorption, *J. Phys. Chem.* 94 (1990) 7119–7128.